



1 **High-time-resolution chemical composition and source apportionment of PM_{2.5} in northern**
2 **Chinese cities: implications for policy**

3 Yong Zhang^{1,2,3}, Jie Tian^{1,2,4}, Qiyuan Wang^{1,2,3,4*}, Lu Qi⁵, Manousos Ioannis Manousakas⁵, Yuemei Han^{1,4}, Weikang
4 Ran^{1,2}, Yele Sun⁶, Huikun Liu^{1,2,4}, Renjian Zhang⁶, Yunfei Wu⁶, Tianqu Cui⁵, Kaspar Rudolf Daellenbach⁵, Jay
5 Gates Slowik⁵, André S. H. Prévôt⁵, Junji Cao^{6*}

6 ¹ State Key Laboratory of Loess and Quaternary Geology, Institute of Earth Environment, Chinese Academy of
7 Sciences, Xi'an 710061, China

8 ² National Observation and Research Station of Regional Ecological Environment Change and Comprehensive
9 Management in the Guanzhong Plain, Shaanxi, Xi'an 710061, China

10 ³ University of Chinese Academy of Sciences, Beijing 100049, China

11 ⁴ Center for Excellence in Quaternary Science and Global Change, Xi'an 710061, China

12 ⁵ Laboratory of Atmospheric Chemistry, Paul Scherrer Institute (PSI), Villigen 5232, Switzerland

13 ⁶ Institute of Atmospheric Physics, Chinese Academy of Sciences, Beijing 100029, China

14 *Correspondence:* wangqy@ieecas.cn (Qiyuan Wang), jjcao@mail.iap.ac.cn (Junji Cao).

15 **Abstract:** Fine particulate matter (PM_{2.5}) pollution is still one of China's most important environmental issues,
16 especially in northern cities during wintertime. In this study, intensive real-time measurement campaigns were
17 conducted in Xi'an, Shijiazhuang, and Beijing to investigate the chemical characteristics and source contributions of
18 PM_{2.5} and explore the formation progress of heavy pollution for policy implications. The chemical compositions of
19 PM_{2.5} in three cities were all dominated by organic aerosol (OA) and nitrate (NO₃⁻). Results of source apportionment
20 analyzed by hybrid environmental receptor model (HERM) showed that the secondary nitrate plus sulfate contributed
21 higher to PM_{2.5} compared to other primary sources. Biomass burning was the dominant primary source in three pilot
22 cities. The contribution of coal combustion to PM_{2.5} is non-negligible in Xi'an and Shijiazhuang but is no longer
23 important contributor in the capital city of Beijing due to the execution of a strict coal-banning policy. The potential
24 formation mechanisms of secondary aerosol in three cities were further explored by establishing the correlations
25 between the secondary nitrate plus sulfate and aerosol liquid water content (ALWC), and O_x (O₃ + NO₂), respectively.
26 The results showed that photochemical oxidation and aqueous-phase reaction were two important pathways of
27 secondary aerosol formation. According to source variations, air pollution events that occurred in campaigns were
28 classified into three types: biomass combustion dominated, secondary nitrate plus sulfate dominated, and a
29 combination of primary and secondary sources. Additionally, this study compared the changes in chemical
30 composition and source contributions of PM_{2.5} in past decades. The results suggested that the clean energy
31 replacements for rural household should be urgently encouraged to reduce the primary source emissions in northern



32 China, and collaborative control on ozone and particulate matter need to be continuously promoted to weaken the
33 atmosphere oxidation capacity for the sake of reducing secondary aerosol formation.

34 **1. Introduction**

35 Fine particulate matter (PM_{2.5}, aerodynamic diameter $\leq 2.5 \mu\text{m}$) is of large concern because of its adverse effects
36 on both natural environment (Kuniyal and Guleria, 2019; Kuo et al., 2013) and human health (Pöschl, 2005; Shen et
37 al., 2021; Zeng and He, 2019). With the soaring economic growth and urbanization in China, PM_{2.5} pollution has
38 been a most serious environmental issue in recent decades (Chan and Yao, 2008; He et al., 2002; Pui et al., 2014;
39 Zhang et al., 2013). The most impressive case is that an extremely severe haze pollution episode occurred in eastern
40 and central China in January 2013 with peak value of PM_{2.5} concentration over $500 \mu\text{g m}^{-3}$. This month had been
41 reported as the haziest month in the past 60 years in Beijing, China (Wang et al., 2014; Huang et al., 2014). Thereafter,
42 aiming to improve air quality, the China central government implemented the Air Pollution Prevention and Control
43 Action Plan (APCAP) in September 2013 (http://www.gov.cn/zwggk/2013-09/12/content_2486773.htm, in Chinese),
44 and the Three-year Action Plan to Fight Air Pollution (TAPFAP) in June 2018
45 (http://www.gov.cn/zhengce/content/2018-07/03/content_5303158.htm, in Chinese). With the implementation of
46 strict pollution controls, air quality in northern China has improved significantly over the past decade (Wang et al.,
47 2020a, 2017; Li et al., 2020). Previous studies show that PM_{2.5} concentration decreased notably in past two decades,
48 and the composition of organic aerosol (OA), black carbon (BC) and sulfate (SO₄²⁻) decreased as well, while the
49 ammonium (NH₄⁺) slightly increased and nitrate (NO₃⁻) increased obviously. In perspective of PM_{2.5} sources,
50 contribution of secondary source increased obviously while contribution of industrial emission and coal combustion
51 decreased due to elimination of industries and enterprises with high pollutant emissions, promotion of desulfurization
52 in industrial facilities, replacement of clean energy, and optimization of industrial and energy structures (Lu et al.,
53 2021; Ma et al., 2022; Tao et al., 2017; Wang et al., 2019). However, there is still a significant gap between the PM_{2.5}
54 concentration in northern China and its latest recommendations on air quality guideline ($5 \mu\text{g m}^{-3}$) by the World
55 Health Organization (<https://apps.who.int/iris/bitstream/handle/10665/345329/9789240034228-eng.pdf>, page 78). In
56 addition, severe PM_{2.5} pollutions still frequently occurred in northern China during wintertime (Guo et al., 2021; Li
57 et al., 2017a, 2021b). To figure out the causes behind the pollutions and improve furtherly air quality in northern
58 China, it is essential to use online high-time-resolution source apportionment technology to understand the chemical
59 composition and source contribution of PM_{2.5} in those pollution events.



60 Recently, more research on measurements of PM_{2.5} and its source apportionments were conducted using online high-
61 time-resolution technologies (Li et al., 2017c; Wang et al., 2021a; Elser et al., 2015). Compared to traditional offline
62 filter-based approach, online methods characterize the short-time variation of PM_{2.5}. It allows for distinguishing the
63 rapid changes and evolutions of chemical components, and is particularly profitable to gain knowledge on the
64 formations of heavy air pollution or episode events (Liu et al., 2016; Ouyang et al., 2019; Zheng et al., 2016; Elser
65 et al., 2015). For instance, Lv et al. (2021) employed a Positive matrix factorization (PMF) model with high-time-
66 resolution online PM_{2.5} data to accurately quantify and distinguish the source distributions in Beijing during two haze
67 episodes in January 2019. Liu et. al (2019) recognized the main drivers of haze event occurred in winter Beijing in
68 2016 according to high-time-resolution source apportionment of PM_{2.5} with multiple models. Furthermore, Wang et
69 al. (2021b) found that vehicle emission contributed most to PM_{2.5} during pollution episodes in downtown Lanzhou
70 based on high-resolution online data source apportionment. Currently, to fully understand and solve heavy pollution
71 events in winter that troubles local governments in northern cities of China (Wang et al., 2022b; Xu et al., 2022; Zhou
72 et al., 2022), more advanced online measurement, and source apportionment is a better choice (Tao et al., 2015). It
73 should be pointed out previous researches were mainly focused on individual cities, and those results have some
74 limitations in guiding the improvement of air quality in the entire northern region of China. Therefore, it is necessary
75 to conduct comparative research among multiple cities.

76 Considering the differences in geographical location, population, economy, industrial/energy structure, air quality,
77 and depth of air pollution control measures among different cities, three cities in northern China including Beijing,
78 Shijiazhuang and Xi'an were chosen as pilot research subjects. The cities of Beijing and Shijiazhuang are located to
79 the North China Plain, which is one of the most polluted regions in China (Chan and Yao, 2008). Beijing is the capital
80 of China and its air quality has significantly improved under the implementation of the strictest clean air policy since
81 2013 (Li et al., 2021a; Pang et al., 2021; Vu et al., 2019; Zhang et al., 2020). However, the city was still plagued by
82 pollution events in wintertime (Wang et al., 2020b; Yang et al., 2022c; Zhou et al., 2022). Shijiazhuang was
83 recognized as one of the most serious air pollution cities worldwide (Liu et al., 2018b; Huang et al., 2019). Its air
84 quality had also improved under the implementation of the Clean Air Plan, whereas its annual PM_{2.5} concentration
85 was still unable to meet the National Ambient Air Quality Standards (NAAQS) until 2021 (Fig. S1). Xi'an is located
86 to the Fenwei Plain, which is a region that suffered from heavy pollution and was designated as a key region for
87 TAPFAP in 2018 (Cao and Cui, 2021). Compared with Beijing and Shijiazhuang, high-intensity air pollution controls
88 in Xi'an started late due to a lack of financial support. And the annual PM_{2.5} concentration in Xi'an could not meet



89 the NAAQS until 2021 as well (Fig. S1). Meanwhile, it is still unclear to the actual causes of the pollution, either
90 topography, meteorological conditions, or local emissions (Chen et al., 2021; Tian et al., 2022; Wang et al., 2015,
91 2022b). In this study, we conducted intensive real-time observation of PM_{2.5} chemical components in Xi'an,
92 Shijiazhuang, and Beijing during wintertime. The objectives are 1) to determine the characteristics of PM_{2.5} and its
93 chemical components in the three typical northern China cities during wintertime; 2) to quantify the source
94 contribution and explore the potential formation mechanism of secondary aerosols; 3) to explore the unique causes
95 of heavy pollution events in different cities; and 4) to provide suggestions on establishment of efficient policies for
96 air quality continuous improvement. This study provides scientific guidance for developing policy on air quality
97 improvement for northern China cities.

98 **2. Methods**

99 **2.1 Sampling sites and periods**

100 In this study, intensive online measurements of PM_{2.5} were conducted at three pilot cities of Xi'an, Shijiazhuang, and
101 Beijing during wintertime (Fig. 1). The sampling sites in Xi'an and Beijing are located at two Chinese Academy of
102 Sciences (CAS) stations. The one in Xi'an is the Guanzhong Plain Ecological Environment Change and
103 Comprehensive Treatment National Observation and Research Station, Institute of Earth Environment (IEE)
104 (34.24°N, 108.87°E), and another one in Beijing is Tower Branch of the Institute of Atmospheric Physics (IAP)
105 (39.98°N, 116.39°E). Both two sites are surrounded by commercial and residential buildings without intense
106 industrial emissions nearby. Previous studies indicated that these two sites were influenced by biomass and coal
107 burning for heating and cooking during wintertime as well as usual local traffic emissions (Tian et al., 2021; Xu et
108 al., 2021). The sampling site in Shijiazhuang is situated in the courtyard of Hebei Sailhero Environmental Protection
109 High-tech Co., Ltd. (38.04°N, 114.65°E), which is surrounded by pharmaceutical and machine-building industries
110 and close to the streets. The intensive campaigns were continuously conducted for ~1 month in each city (i.e., 12
111 December 12th 2020 to January 7th 2021 in Xi'an, December 20th 2021 to January 24th 2022 in Shijiazhuang, and
112 January 17th 2021 to February 20th 2021 in Beijing).

113 **2.2 Online measurements of PM_{2.5} chemical components**

114 **2.2.1 Organic aerosol and inorganic ions**

115 Concentrations of OA, NO₃⁻, SO₄²⁻, ammonium (NH₄⁺), and chloride (Cl⁻) in PM_{2.5} at a 15-minute time resolution



116 were monitored by a quadrupole aerosol chemical speciation monitor (Q-ACSM, Aerodyne Research Inc., Billerica,
117 Massachusetts, USA) equipped with a PM_{2.5} lens. The detailed operational principles and calibration method of the
118 Q-ACSM are described elsewhere (Ng et al., 2011; Hu et al., 2017). First, the sampled ambient air stream passed
119 through a PM₁₀ impactor inlet and a Nafion[®] dryer (MD-700-24F-3; Perma Pure, Inc., Lakewood, NJ, USA) with a
120 flowrate of 5 L min⁻¹ before entering the Q-ACSM chamber. Then, the pre-treatment particles passed through a 100
121 μm critical orifice at 0.1 L min⁻¹ and were focused into a narrow beam by an aerodynamic intermediate pressure lens.
122 The focused particle beam was flash vaporized by a capture vaporizer (CV) at ~600 °C. The vaporized compounds
123 were then ionized by an electron impactor (EI) ionization source at 70 eV and subsequently analyzed by the
124 quadrupole mass spectrometer.

125 Based on calibration system consists of an atomizer (Model 9302, TSI Inc., Shoreview, MN, USA), a differential
126 mobility analyzer (DMA, TSI model 3080, TSI Inc.), and a condensation particle counter (CPC, TSI model 3772,
127 TSI Inc.), ammonium nitrate (NH₄NO₃) and ammonium sulfate ((NH₄)₂SO₄) aerosol were used for calibration. The
128 raw data of Q-ACSM were analyzed by the ACSM local tool (V1.5.3.5, Aerodyne Research Inc., Billerica,
129 Massachusetts, USA) compiled with Igor Pro 6.37 (Wavemetrics, Lake Oswego, OR, USA). The response factors
130 (RFs) for NO₃⁻ in Xi'an, Shijiazhuang, and Beijing were set as 2.03×10⁻¹¹, and 5.9×10⁻¹¹, 2.20×10⁻¹¹, respectively,
131 and the relative ionization efficiencies (RIEs) for NH₄⁺ and SO₄²⁻ were set as 8.06 and 0.83 in Xi'an, 5.82 and 0.30
132 in Shijiazhuang, 6.31 and 0.38 in Beijing, respectively. Other RIEs for NO₃⁻, OA, and Cl⁻ were set as default values
133 of 1.4, 1.1, and 1.3, respectively (Ng et al., 2011). In addition, the collection efficiency (CE) value of Q-ACSM
134 equipped with a PM_{2.5} lens was recommended as 1 based on laboratory simulation experiments by Xu et al. (2017).
135 Finally, the chemical components monitored by Q-ACSM was corrected by the results of offline filter sampling
136 experiments during the same periods (Fig. S2).

137 **2.2.2 Black carbon**

138 BC concentration in PM_{2.5} was obtained by an Aethalometer (Model AE33, Magee Scientific Inc., Berkeley, CA,
139 USA) with a 1-minute time resolution. The AE33 monitors the light attenuation of seven wavelengths (λ = 370, 470,
140 525, 590, 660, 880, and 940 nm), and the light attenuation at λ = 880 nm was used to calculate BC concentration
141 (Wang et al., 2019; Drinovec et al., 2015). Briefly, the ambient air was first sampled on a filter tape inside the
142 instrument through a PM_{2.5} cyclone (SCC-1.829, BGI Inc., USA) at a flowrate of 5 L min⁻¹. The entering particles
143 were divided into two sample spots on the filter through two channels with different follows. Then the light



144 attenuation transmitted through two parallel spots was detected. For quality accuracies of monitoring, the sampled
145 particles were desiccated with a Nafion[®] dryer (MD-700-24F-3; Perma Pure, Inc., Lakewood, NJ, USA) before
146 entering the AE33. Furthermore, a real-time loading effect compensation algorithm based on two spots measurement
147 was used to eliminate the nonlinear loading effects of the Aethalometer. A detailed description of the Model AE33
148 principle can be found in Drinovec et al. (2015).

149 **2.2.3 Elements**

150 Twenty-four elements, including Si, K, Ca, V, Cr, Mn, Fe, Co, Ni, Cu, Zn, Ga, As, Se, Ag, Cd, Sn, Ba, Au, Hg, Th,
151 Pb, and Pd in PM_{2.5}, were analyzed by a Xact625 Ambient Metals Monitor (Cooper Environmental Services, Tigard,
152 Oregon, USA) with a 1-hour time resolution. Si, K, Ca, Cr, Mn, Fe, Ni, Cu, Zn, As, Se, Ba, and Pb were selected for
153 further analysis in Xi'an and Beijing, while other elements were excluded due to most of their concentration below
154 the method detection limit. In Shijiazhuang, S, Cl, and Ti were analyzed by replacement of Ga, Ag and Au,
155 respectively. Finally, Si, K, Ca, Ti, Cr, Mn, Fe, Ni, Cu, Zn, As, Se, Ba, and Pb were selected for further analysis. The
156 description and detection principles of Xact625 were introduced by Furger et al. (2020) and Rai et al. (2020). In brief,
157 the ambient air stream was firstly sampled on a Teflon filter tape inside the instrument through a PM_{2.5} cyclone inlet
158 at a constant flow rate of 16.7 L min⁻¹, and then the sample was automatically analyzed by nondestructive energy-
159 dispersive X-ray fluorescence (XRF) to determine the mass of the species. For quality control and assurance, the
160 Xact625 performed automatic internal quality control by testing the Pd rod every hour to ensure the stability of the
161 instrument. Energy calibration was performed daily from 00:00 to 00:15 and a range calibration from 00:15 to 00:30
162 local standard time (LST) to monitor any possible shift and instability of the XRF (Liu et al., 2019). During our
163 sampling periods, the concentration of Pd varies within 3 standard deviations (Fig. S3), illustrating the reliable and
164 stable performance of the Xact625.

165 **2.2.4 Complementary data**

166 Online hourly concentrations of PM_{2.5} and gas pollutants (i.e., NO_x, NO₂, CO, SO₂, and O₃) were acquired from the
167 National Air Quality Monitoring Station (<https://air.cnemc.cn:18007/>). Meteorological parameters, including wind
168 speed (WS), wind direction (WD), relative humidity (RH), and temperature (T) were obtained from National
169 Meteorological Station (<http://data.cma.cn/>). The detailed information for complementary data was listed in Table S1.

170 **2.3 Data analysis**



171 2.3.1 PM_{2.5} mass reconstruction

172 Chemical closure was utilized to assess whether chemical compositions can be representative of PM_{2.5}. The sum of
173 OA, NO₃⁻, SO₄²⁻, NH₄⁺, Cl⁻, BC, mineral dust (MD), and trace elements (TE) was considered as the reconstructed
174 PM_{2.5}, where MD and TE were calculated as follows (Chow et al., 2015).

$$175 \text{ [MD]} = 2.20 \times [\text{Al}] + 2.49 \times [\text{Si}] + 1.63 \times [\text{Ca}] + 2.42 \times [\text{Fe}] + 1.94 \times [\text{Ti}] \quad (1)$$

$$176 \text{ [TE]} = [\text{K}] + [\text{Cr}] + [\text{Mn}] + [\text{Ni}] + [\text{Cu}] + [\text{Zn}] + [\text{As}] + [\text{Se}] + [\text{Ba}] + [\text{Pb}] \quad (2)$$

177 where [] represents the chemical species concentration; [Al] and [Ti] were calculated by the concentration of Ca
178 ([Al] = 4.3 × [Ca] and [Ti] = 0.25 × [Ca]) (Wei et al., 1991). Good correlations between online and reconstructed PM_{2.5}
179 mass (slope = 0.87–1.10, R² = 0.82–0.93) in three pilot cities (Fig. S4) indicated that our measurements could detect
180 major components of PM_{2.5}. The PM_{2.5} concentration used in the following discussion referred to the reconstructed
181 PM_{2.5} concentration.

182 2.3.2 Hybrid environment receptor model

183 Source apportionment of PM_{2.5} was analyzed with a bilinear model named the hybrid environment receptor model
184 (HERM). HERM is developed by the IEECAS and the University of Nevada, Las Vegas (Chen and Cao, 2018). Like
185 other receptor models, the speciation of pollutants at a receptor site can be separated into emission sources and the
186 chemical compositions of the sources. To solve the mass balance of PM_{2.5}, the bilinear HERM in matrix notation is
187 defined as follows

$$188 C_{mn} = \sum_{i=1}^I F_{mi} G_{in} + Q_{mn} \quad (3)$$

189 where C_{mn} is the measured concentration of chemical species m during time n ; F_{mi} is the source profile, that is the
190 fractional quantity of species m in source i emission; G_{in} represents the contribution of source i during time n ; and
191 Q_{mn} is the model residual for species m concentration measured during time n . Based on an iterative conjugate
192 gradient algorithm, the HERM solves G_{in} and unknown F_{mi} by minimizing the Q_{mn} , which is defined as follows.

$$193 Q_{mn} = \sum_{m=1}^M \sum_{n=1}^N \frac{(C_{mn} - \sum_{i=1}^I F_{mi} G_{in})^2}{\sigma_{mn}^2 + \sum_{i=1}^I (\sigma_{mi}^2 G_{in}^2 + \delta_{mi} \sigma_{mn}^2)} \quad (4)$$

194 where M , N , and I are the number of samples, chemical species, and sources, respectively; $\sigma_{F_{mi}}$ represents the error
195 in the variability in the constrained factor profile. δ_{mi} was set to 0 or 1 depending on whether the i^{th} factor profile
196 is constrained or unconstrained, respectively.

197 The HERM input data included the concentration and uncertainty data of chemical species. 19 chemical species in



198 Xi'an and Shijiazhuang and 20 chemical species in Beijing were selected for source apportionment, respectively.
199 Details of selected chemical species and its uncertainty calculation was described in Text S1 in the Supplement. A
200 range from two to ten factors solutions was investigated by HERM with completely unconstrained factor profiles to
201 search for optimal solutions. The detailed diagnostics can be seen in Text S2 in the Supplement. A six-factor solution
202 for Xi'an and Shijiazhuang and an eight-factor solution for Beijing were found to be the optimal solution based on
203 multiple criteria including 1) variations in Q/Q_{exp} which can be used to choose the optimal number of resolved factors,
204 2) physical meaningfulness of distinct factor profiles and explained variation (EV) values of variables, 3) good
205 correlations between sources contribution and external and internal tracers, and 4) agreement between the measured
206 and modeled $\text{PM}_{2.5}$ mass. More detailed information on the final selected factor profiles and contributions is presented
207 in Sect. 3.2.

208 2.3.3 Aerosol liquid water content

209 Aerosol liquid water content (ALWC) was calculated by ISORROPIA-II thermodynamic equilibrium model
210 (<http://isorrophia.eas.gatech.edu/>) based on data of $\text{PM}_{2.5}$ chemical species (including NO_3^- , SO_4^{2-} , NH_4^+ , and Cl^-) and
211 meteorological parameters including relative humidity (RH) and temperature (T), more model information can be
212 found in Fountoukis and Nenes (2007). It should be noted that the ISORROPIA-II model does not consider the
213 contribution of the organic, as inorganic aerosols are the most hygroscopic species and dominant contributor to
214 ALWC (Huang et al., 2020).

215 3. Results and discussion

216 3.1 Characteristics of $\text{PM}_{2.5}$ and its chemical components

217 Figure 1 illustrates the mass composition of $\text{PM}_{2.5}$ in three pilot cities during the sampling periods, and their
218 concentrations levels are summarized in Table S4. The average $\text{PM}_{2.5}$ concentrations in Xi'an, Beijing, and
219 Shijiazhuang were $77 \pm 47 \mu\text{g m}^{-3}$, $64 \pm 57 \mu\text{g m}^{-3}$, and $60 \pm 39 \mu\text{g m}^{-3}$, respectively. It is noted that the average $\text{PM}_{2.5}$
220 concentrations in Xi'an, Beijing, and Shijiazhuang did not meet the second level of the NAAQS, indicating that it is
221 necessary to establish more particular and efficient pollution reduction measures. As shown in Fig. 1, the chemical
222 compositions of $\text{PM}_{2.5}$ were similar in Beijing and Shijiazhuang (Fig. 1b and c) which was mainly composed of OA
223 (26.9–34.2%), followed by NO_3^- (23.6–26.5%), SO_4^{2-} (11.8–15.0%), NH_4^+ (11.8–14.8%), MD (7.4–10.1%), BC (2.9–
224 6.5%), and Cl^- (1.1–4.8%). However, in Xi'an, MD contributed in comparison more to $\text{PM}_{2.5}$ (17.3%), while SO_4^{2-}



225 had a smaller contribution (6.8%). This could be explained by more construction activities and MD transport from
226 the Loess Plateau to Xi'an (Long et al., 2016; Yan et al., 2015). Meanwhile, the lowest sulfur oxidation ratio (SOR)
227 was observed in Xi'an (0.18 ± 0.08 , see Table S5), indicating weak efficiency of the second generation of SO_4^{2-} . The
228 sum of SO_4^{2-} , NO_3^- and NH_4^+ accounted for 39.0–53.0% of $\text{PM}_{2.5}$ in three pilot cities, highlighting the importance of
229 the secondary inorganic components in northern China. In addition, the fractions of BC, Cl^- , and TE in $\text{PM}_{2.5}$ were
230 lower in Beijing than those in the other two cities, which can be explained by the stricter local control policies on
231 solid fuels combustion and tightening the industrial emission standards in and near the capital city of China (Li et al.,
232 2021a; Pang et al., 2021).

233 To have a better understanding of the impact of the chemical components, the mass fraction of each component was
234 plotted as a function of the $\text{PM}_{2.5}$ mass concentration (Fig. 2a–c). The two dominant components of $\text{PM}_{2.5}$ were OA
235 (25.7–38.0%) and MD (19.9–37.1%) while the $\text{PM}_{2.5}$ concentrations were below $40 \mu\text{g m}^{-3}$. The fraction of OA in
236 $\text{PM}_{2.5}$ was the highest in Shijiazhuang and Beijing, while MD contributed most to $\text{PM}_{2.5}$ in Xi'an. This is potentially
237 related to more emissions and higher backgrounds of local dust. With increasing of the $\text{PM}_{2.5}$ mass concentration, the
238 fractions of chemical components in Xi'an and Shijiazhuang changed notably. The fractions of OA and NO_3^- increased
239 the most and reached the peaks of 40.1% and 28.7%, respectively, when the $\text{PM}_{2.5}$ concentration reached $\sim 196 \mu\text{g m}^{-3}$
240 in Xi'an. On the contrary, NO_3^- and SO_4^{2-} were two dominant drivers of increasing $\text{PM}_{2.5}$ concentrations in
241 Shijiazhuang, showing peak contributions of 32.5% and 18.7%, respectively, when the $\text{PM}_{2.5}$ concentration was over
242 $100 \mu\text{g m}^{-3}$. Compared to Xi'an and Shijiazhuang, Beijing had relatively stable fractions of each chemical component
243 with increasing $\text{PM}_{2.5}$ concentrations. Particularly, the fractions of OA and NO_3^- contributed dominantly with
244 averages of $33.3 \pm 3.0\%$ and $25.3 \pm 2.5\%$, respectively, when the $\text{PM}_{2.5} > 40 \mu\text{g m}^{-3}$.

245 3.2 Source apportionment of $\text{PM}_{2.5}$

246 Six potential sources, including biomass burning, fugitive dust, industrial emission, coal combustion, vehicle
247 emission, and secondary nitrate plus sulfate, were resolved by the HERM analysis. In Beijing, secondary nitrate plus
248 sulfate was furtherly divided into secondary nitrate and secondary sulfate. A special pollution source of firework was
249 separated due to the Chinese Spring Festival (from New Year's Eve to January 3rd in the lunar calendar). Figures S6–
250 S8 present the sources profiles and contributions in Xi'an, Shijiazhuang, and Beijing, respectively. Biomass burning
251 features high Explained Variation (EV) for the two tracers Cl^- (33–58%) and K (30–44%) in the three cities (Ni et al.,
252 2017; Zhao et al., 2021). The fugitive dust is characterized by high EV values for Si (60–90%) and Ca (34–54%),



253 which are the dominant chemical species in the fugitive dust profiles in northern China (Shen et al., 2016; Zhao et al., 2006). The fractions of industrial emission vary among the cities, showing high EV for Ni (55% and 87%) and 254 al., 2006). The fractions of industrial emission vary among the cities, showing high EV for Ni (55% and 87%) and 255 Cr (25% and 70%) in Xi'an and Shijiazhuang, and high EV for Cr (26%), Mn (40%), and Pb (27%) in Beijing. Ni is 256 possibly emitted from the semiconductor industry (Simka et al., 2005). Cr, Mn, and Pb could originate from the steel 257 manufacturing and incinerator fly ash (Duan and Tan, 2013; Ledoux et al., 2017). Coal combustion is characterized 258 by high EV values for As (38–75%), Se (40–50%), and Pb (31–57%). These elements are enriched in coals, which 259 are reliable indicators of coal combustion (Tian et al., 2013; Xu et al., 2012). The vehicle non-exhaust emissions 260 could be identified by the elements Ba, Cu, Ca, Fe, and Mn. Cu and Ba can be released from brake and tire wear of 261 vehicles (Adachi and Tainosho, 2004; Thorpe and Harrison, 2008). Moreover, Fe and Mn could be emitted from the 262 combustion of lubricating oil and fuel additives (Ålander et al., 2005; Lewis et al., 2003). Relatively high EV values 263 for Ba (68%), Cu (36%), and Ca (35%) are seen in Xi'an, significantly high EV values of Mn (68%), Fe (65%), Cu 264 (53%), and Ba (80%) are characterized in Shijiazhuang and relatively high EV values of Fe (34%) and Cu (39%) are 265 featured in Beijing, respectively. Moreover, moderate EV values for BC (18–27%) and OA (13–22%) are commonly 266 regarded as contributions of vehicles engine exhaust, while the temporal variations of VE are well correlated with 267 gaseous NO_x or NO_2 in three cities ($R^2 = 0.45\text{--}0.78$), which is the good tracer of traffic-related emissions (Huang et 268 al., 2017; Li et al., 2017b). The secondary sources resolved by HERM are different among the three cities. In Xi'an 269 and Shijiazhuang, the source of secondary nitrate plus sulfate are characterized by high EV values for SO_4^{2-} (62– 270 75%), NO_3^- (55–53%), NH_4^+ (60–56%), which showed good correlations with SO_4^{2-} ($R^2 = 0.85\text{--}0.90$) and NO_3^- ($R^2 271 = 0.85\text{--}0.92$) (Dai et al., 2020; Tian et al., 2022). In Beijing, the secondary sources of nitrate and sulfate show high 272 EV values of 58% and 65%, respectively. The combination of secondary nitrate and secondary sulfate is equivalent 273 to the secondary nitrate plus sulfate for next discussion. Additionally, the source of firework emission is characterized 274 by high EV values of Ba (83%), Cu (45%), and K (38%), which are recognized as common indication in fireworks 275 (Rai et al., 2020; Tian et al., 2014).

276 The modeled $\text{PM}_{2.5}$ mass was well correlated with the reconstructed $\text{PM}_{2.5}$ mass ($R^2 = 0.99$, slope = 0.90–1.01, Fig. 277 S9) in three pilot cities, indicating the established models are reasonable. As shown in Fig. 1d and e, the contributions 278 of primary sources (i.e., the sum of biomass burning, fugitive dust, industrial emission, coal combustion, and vehicle 279 emission) in $\text{PM}_{2.5}$ were significantly higher than those of the source of secondary nitrate plus sulfate in Xi'an and 280 Shijiazhuang, indicating the $\text{PM}_{2.5}$ in these two cities are mainly influenced by the primary source emissions during 281 wintertime. Particularly, biomass burning and coal combustion were two dominant contributors to $\text{PM}_{2.5}$ with



282 contributions of 24.6% and 15.1%, respectively, in Xi'an; and 24.4% and 16.0%, respectively, in Shijiazhuang. These
283 suggest that controls of solid fuel combustion are critical to reducing PM_{2.5} pollution in these cities. In contrast, the
284 contribution of secondary nitrate plus sulfate to PM_{2.5} in Beijing was highly dominant (> 50%), potentially attributed
285 to strict control of primary emissions under the execution of a series of pollution control policies (Lv et al., 2016;
286 Pang et al., 2021), and more regional transportation of secondary pollutants (Liu et al., 2019; Wang and Zhao, 2018).
287 Among the primary sources, the contributions of biomass burning and vehicle emission were only 18.4% and 11.3%,
288 respectively, further reflecting the benefits of reductions of all primary emissions. Due to the Chinese Spring Festival,
289 the contribution of firework (7.9%) to PM_{2.5} ranked second in primary sources (Fig. S10). Which indicates more
290 refined control schemes need to be encouraged to deal with such special event in the future. It should be note that
291 contribution of fugitive dust was all lower than fraction of mineral dust in the three pilot cities (Fig. 1). This is because
292 fugitive dust defined here mainly refers road and construction dust emission. While mineral dust represents material
293 assumed oxides of mineral elements such as Al, Si, Ca, Ti and Fe (Chow et al., 2015). These mineral elements in
294 PM_{2.5} comes from more emission sectors including industry, crust, and transportation, construction, combustion (Liu
295 et al., 2018a; Lu et al., 2014; Pant and Harrison, 2013; Shen et al., 2016).

296 Figures 2d–f shows variations of source contribution with increases in PM_{2.5} mass concentrations in three pilot cities.
297 The most two dominant sources were secondary nitrate plus sulfate (32.1%) and fugitive dust (31.4%) in Xi'an, coal
298 combustion (24.9%) and vehicle emission (21.3%) in Shijiazhuang, and secondary nitrate plus sulfate (24.3%) and
299 fugitive dust (23.8%) in Beijing, when the PM_{2.5} mass concentration <40 µg m⁻³. In Xi'an, when the PM_{2.5} mass
300 concentrations exceeded 180 µg m⁻³, the contribution of biomass burning raised mostly and reached the peak of
301 38.4%, demonstrating that biomass burning plays an important role in worsening of air quality in Xi'an. On the
302 contrary, the contributions of secondary nitrate plus sulfate increased mostly in comparison to other sources in
303 Shijiazhuang and Beijing, indicating the PM_{2.5} pollution was mainly dominated by the secondary aerosol formations
304 during the wintertime. And the peak contributions of secondary nitrate and sulfate were 66.5% and 74.7% while the
305 PM_{2.5} mass concentration increased to 113 µg m⁻³ and 223 µg m⁻³ in Shijiazhuang and Beijing, respectively.

306 **3.3 Formation of secondary aerosols**

307 Using the high-time-resolution data, we further explored the possible formation mechanisms of secondary nitrate
308 plus sulfate. The concentration of secondary nitrate plus sulfate is standardized by dividing background corrected CO
309 (ΔCO) to weaken impact of planetary boundary layer height (PBLH) (DeCarlo et al., 2010). In this study, ΔCO is



310 defined as the 1.25th percentile of CO concentration during the campaign, which are 0.17, 0.15, and 0.16 ppm in
311 Xi'an, Shijiazhuang, and Beijing, respectively. O_x ($NO_2 + O_3$) is an indicator of the photochemical oxidation degree
312 (Wood et al., 2010). The function between secondary nitrate plus sulfate/ ΔCO ratio and O_x during the daytime (i.e.,
313 08:00–17:00 LST) (Fig. S11) was plotted to explain the effect of photochemical oxidations in three pilot cities. As
314 shown in Fig. 3, good linear correlations of secondary nitrate plus sulfate/ ΔCO and O_x ($R^2 = 0.83$ – 0.99) suggest that
315 photochemical oxidations play an important role in the formation of secondary aerosol during the daytime. Compared
316 to the low-level O_x , formation of secondary aerosol significantly enhanced at high-level O_x (>50 ppb) in Xi'an and
317 Beijing, characterized by larger slopes of 17.2 and 38.9, respectively (Fig. 3a and c). Furthermore, the highest
318 atmospheric oxidation capacity was found in Beijing, inferring by the highest fraction of O_3 to O_x . This is consistent
319 with the highest contribution of secondary nitrate plus sulfate to $PM_{2.5}$ in Beijing during the daytime (Fig. S12a–c).

320 The aqueous-phase reaction is another important pathway for secondary aerosol formation in the atmosphere (Wang
321 et al., 2018; Xue et al., 2014). ALWC is considered an indicator of an aqueous-phase reaction (Ervens et al., 2011).
322 The correlations of secondary nitrate plus sulfate/ ΔCO ratio and ALWC during nighttime (18:00–07:00 the next day
323 LST, Fig. S11) were established in three pilot cities to assess the implications of aqueous-phase chemistry for
324 secondary aerosol production. The secondary nitrate plus sulfate/ ΔCO showed a significant linear correlation to
325 ALWC ($R^2 = 0.81$ – 0.95) when $RH < 80\%$ (Fig. 4), indicating an obvious effect of aqueous-phase reaction on the
326 secondary aerosol formation during the nighttime. However, when $RH > 80\%$, the secondary nitrate plus sulfate/ ΔCO
327 showed no notable increase with ALWC in Shijiazhuang (Fig. 4b), whereas a tiny increase with ALWC in Beijing
328 (Fig. 4c). The higher ALWC at $RH > 80\%$ probably inhibits secondary aerosol formation due to the decrease in
329 aerosol acidity (Huang et al., 2019; Meng et al., 2014). Khan et al. (2008) found that NO_3 radicals can rapidly generate
330 from the reaction between NO_2 and O_3 with unsaturated organic species during nighttime. The value of $O_3 \times NO_2$ can
331 thus represent its production reaction rate or be used as a proxy for the NO_3 radical. The highest NO_3 radical
332 production rate was found in Beijing, followed by Xi'an and Shijiazhuang, when $RH < 80\%$. This could be used to
333 explain the highest contribution of secondary nitrate plus sulfate to $PM_{2.5}$ in Beijing during the nighttime (Fig. S12d–
334 f). Moreover, the results showed that both photochemical oxidation and aqueous-phase reaction play more important
335 roles in Beijing, where the primary sources have been better controlled. This reflects that pollution control policies
336 need to be focused on the suppression of secondary formations.

337 3.4 Elaborations of different episode cases



338 During the sampling periods, the concentration of $PM_{2.5}$ and its chemical components simply accumulated within a
339 short period in a few cases (Fig.S13a-c). We define such a rapid rise in $PM_{2.5}$ mass concentration as a pollution
340 episode. As shown in Table 1, meteorological conditions, concentration levels of gas pollutants, chemical
341 compositions, and source contributions of $PM_{2.5}$ during pollution episodes in three pilot cities are summarized. The
342 episodes were accompanied by low wind speed ($< 2 \text{ m s}^{-1}$), leading to weak dispersions of the fresh emissions and
343 accumulated pollutants (Chen et al., 2020b). The two dominant chemical components in $PM_{2.5}$ during all pollution
344 episode cases were OA and NO_3^- , with fractions of 26–40% and 23–32%, respectively. Their high abundances could
345 be explained by the significant reduction of SO_2 emissions by the prohibiting of burning bulk coals and executing
346 the “Coal-to-Natural Gas” policy in recent years (Meng et al., 2022). In this study, eight pollution episodes (donated
347 as EP1-EP8) were classified into three types: The first type was dominated by biomass burning (30–40%) (EP1, EP4,
348 and EP8). The second type was dominated by secondary nitrate plus sulfate (61–70%) (EP5, EP6, and EP7). The two
349 remaining pollution episodes were mutually contributed by both primary and secondary sources (EP2 and EP3), in
350 which secondary nitrate plus sulfate (34–39%) and biomass burning (23–24%) were the two dominant contributors
351 to $PM_{2.5}$.

352 To profoundly understand the progress of pollution episodes, three typical pollution events were chosen for detailed
353 discussion (i.e., EP2 in Xi’an, EP4 in Shijiazhuang, and EP7 in Beijing) based on the validity and integrity of the
354 data and the representativeness of the selected pollution events. For the first type of episode represented by EP4 (Fig.
355 S14), a two-stages evolution was distinguished. At Stage 1, the $PM_{2.5}$ mass concentrations rapidly increased from 7
356 to $82 \mu\text{g m}^{-3}$ under stable weather conditions inferring by low wind speed ($1.8 \pm 0.8 \text{ m s}^{-1}$, Fig. S14b), in which the
357 concentrations (fractions) of biomass burning increased from $0.6 \mu\text{g m}^{-3}$ (7%) to $36.7 \mu\text{g m}^{-3}$ (55%) due to heating
358 demand during nighttime. Meanwhile, the chemical composition was relatively stable and dominated by OA ($31 \pm 5\%$)
359 and NO_3^- ($21 \pm 5\%$). At Stage 2, the $PM_{2.5}$ mass concentration continuously increased to $105 \mu\text{g m}^{-3}$ in a few hours
360 along with the most notable abundance of the source of secondary nitrate plus sulfate, which concentration
361 (contribution) rapidly increased from $2.3 \mu\text{g m}^{-3}$ (4%) to $54.4 \mu\text{g m}^{-3}$ (52%) (Fig. S14g and h). This is due to the
362 aqueous-phase reactions effect inferring by the rapid increase in ALWC (from $16 \mu\text{g m}^{-3}$ to $78 \mu\text{g m}^{-3}$, Fig. S14c) and
363 RH (from 51% to 79%, Fig. S14a).

364 In contrast, a three-stages evolution was discriminated for the second type of episode, using EP7 as an example (Fig.
365 S15). At Stage 1, the $PM_{2.5}$ concentration gradually increased from 11 to $30 \mu\text{g m}^{-3}$, as well as NO_2 (from 15 to 59



366 $\mu\text{g m}^{-3}$, Fig. S15d) due to the boosts of predominant contributions of vehicle emission and biomass burning (Fig.
367 S15g and h). In the meantime, the contribution of coal combustion also slowly increased along with SO_2 (Fig. S15d
368 and h). At Stage 2, under the lowest average wind speed ($0.7\pm 0.4 \text{ m s}^{-1}$, Fig. S15b), the $\text{PM}_{2.5}$ mass concentrations
369 moderately increased from 30 to $91 \mu\text{g m}^{-3}$ with relatively stable chemical composition and source contribution (Fig.
370 S15f and h). Compared to Stage 1, the fractions of NO_3^- increased mostly from $9\pm 3\%$ to $23\pm 3\%$, this is probably
371 influenced by photochemical oxidations inferring by relative high O_x and NO_2 concentration (Fig. S15c and d). At
372 Stage 3, the $\text{PM}_{2.5}$ mass concentration rapidly rose to $142 \mu\text{g m}^{-3}$ and then remained stable. In which the
373 concentrations (fractions) of secondary nitrate plus sulfate increased mostly from $18.9 \mu\text{g m}^{-3}$ (48%) to $120.6 \mu\text{g m}^{-3}$
374 (80%). This might be due to the occurrence of an aqueous-phase reaction, which was indicated by the elevation of
375 RH and ALWC (Fig. S15a and c).

376 Figure S16 illustrates the third type of episode using EP2 as an example, while a four-stages evolution was resolved.
377 At Stage 1, the $\text{PM}_{2.5}$ mass concentration ($14\pm 3 \mu\text{g m}^{-3}$) was relatively low and dominated by the contributions of
378 secondary nitrate plus sulfate ($43\pm 17\%$) and fugitive dust ($24\pm 8\%$), as well as MD ($28\pm 7\%$) and OA ($26\pm 7\%$). At
379 Stage 2, the $\text{PM}_{2.5}$ mass concentrations promptly increased from 21 to $82 \mu\text{g m}^{-3}$, with the two dominant chemical
380 components of OA ($21.7 \mu\text{g m}^{-3}$) and NO_3^- ($17.1 \mu\text{g m}^{-3}$). The $\text{PM}_{2.5}$ increases can be also contributed to the raise of
381 secondary nitrate plus sulfate ($25.3 \mu\text{g m}^{-3}$) and biomass burning ($14.4 \mu\text{g m}^{-3}$). The enhancement of secondary aerosol
382 was probably generated through the aqueous-phase reaction evidenced by the increase of ALWC and NO_2 (Fig. S16c
383 and d). At Stage 3, $\text{PM}_{2.5}$ mass continuously increased to $139 \mu\text{g m}^{-3}$ with dominant increase of primary sources
384 emission including biomass burning ($29.0 \mu\text{g m}^{-3}$), vehicle emission ($21.5 \mu\text{g m}^{-3}$) and coal combustion ($16.5 \mu\text{g m}^{-3}$)
385 along with increase of SO_2 and NO_2 as well (Fig. S16 d). The three primary sources contributed $>60\%$ of the total
386 resolved sources. Meanwhile, the secondary nitrate plus sulfate also increased slowly through aqueous-phase reaction
387 inferring by increase of ALWC (Fig. S16c). At the final Stage 4, the $\text{PM}_{2.5}$ mass concentration maintained relatively
388 stable with an average of $142\pm 11 \mu\text{g m}^{-3}$, dominated by sources of secondary nitrate plus sulfate ($34\pm 6\%$) and biomass
389 burning ($28\pm 6\%$); and chemical components of OA ($36\pm 4\%$) and NO_3^- ($25\pm 1\%$).

390 In summary, the pollution event occurred in Xi'an was mainly derived by stronger emissions of primary sources
391 under adverse meteorological conditions, even though the aqueous-phase reaction also contribute to secondary
392 aerosol formation. In contrast, pollution events occurred in Shijiazhuang and Beijing were mainly influenced by
393 formation of secondary aerosols through both of aqueous-phase reaction and photochemical oxidation. What's more,



394 in which aqueous-phase reaction plays more important role than photochemical oxidation. Hence, to further improve
395 the air quality in the north of China, primary source emissions should be prioritized for control in the northwest
396 region, with a focus on biomass burning and coal combustion. In the North China Plain, priority should be given to
397 reducing emissions of precursors from secondary sources, with a focus on NO_x and volatile organic compounds
398 (VOCs).

399 **3.5 Policy implications**

400 In past decades, the air quality in China improved notably under the implementation of air pollution control policies
401 including APCAP and TAPFAP. The $\text{PM}_{2.5}$ mass in Xi'an, Shijiazhuang and Beijing were the lowest during campaigns
402 compared with those in last decades (Table S6). The variations of the chemical composition and the source
403 contribution of $\text{PM}_{2.5}$ in the three pilot cities are displayed in Fig. 5. As shown, the dominant chemical components
404 of $\text{PM}_{2.5}$ changed from OA and SO_4^{2-} , to OA and NO_3^- (Fig. 5a–c). This could be attributed to the reduction in coal
405 consumption due to clean energy replacement and the increase of vehicle ownership. This led a decrease of the SO_2
406 and an increase of NO_2 (Wang et al., 2013). Since the atmospheric oxidation reaction (i.e., aqueous-phase reaction
407 and photochemical oxidation) of the precursors (i.e., NO_2 , VOCs) is the primary source for the OA and NO_3^- in the
408 atmosphere (Feng et al., 2018; Li et al., 2022; Tao et al., 2016; Yang et al., 2022b; Ziemann and Atkinson, 2012), and
409 it is impossible to avoid, thus, the precursors of OA and NO_3^- should be reduced from the combustion and
410 transportation sectors (Fermo et al., 2021; Liu et al., 2022; Wang et al., 2021c; Zhang et al., 2019). In addition, the
411 fraction of NH_4^+ in $\text{PM}_{2.5}$ increased with an alarming rate. This is coincidentally in a similar trend of NH_3 . Studies
412 have reported that controls of NH_4^+ is more effective than that of NO_x in the reduction of $\text{PM}_{2.5}$ mass concentrations
413 (Gu et al., 2021; Zheng et al., 2022). Therefore, collaborative control measures for the emissions of precursors
414 including NO_x , VOCs, and NH_3 are necessary.

415 As shown Table S7 and Fig. 5d-f, coal combustion decreased remarkably due to the coal-related policies
416 implementation including the strength of emissions standards for coal-fired power plants, the change of energy
417 sources from coal to natural gas in some industrials, and the coal burning was forbidden in the main urban areas
418 (Shen, 2016; Yang and Teng, 2018). Meanwhile, the contribution of industrial emission and vehicle emission
419 decreased slightly because of the improvement of industrial emission standards (He et al., 2020; Wang et al., 2020a)
420 and the traffic-related policy implementation such as the strength of vehicle emission standards, improvement of fuel
421 quality, and elimination of high-emission-vehicles. This resulted in the reduction of the precursor gases and $\text{PM}_{2.5}$



422 from vehicles (Feng et al., 2021; Fontaras et al., 2012; Jin et al., 2012). However, the emission of biomass burning
423 did not show a significant reduction in recent years, and its contribution increased from 9% in 2014 to 25% in 2020
424 (Xi'an), from 3% in 2015 to 24% in 2022 (Shijiazhuang), and from 6% in 2013 to 18% in 2021 (Beijing) (Fig. 5d-f).
425 This is likely because biomass burning is an open source, which makes it more difficult to control compare with other
426 primary sources. Biomass used for residential heating in rural areas is still frequently occurred (Ren, 2021; Tian et
427 al., 2022; Yang et al., 2022a; Zhang et al., 2017). Hence, the clean energy revolution should be promoted urgently
428 especially in the entire regions in northwest China. Moreover, the contributions of secondary sources increased, it is
429 potentially explained by the high reduction rate of primary emissions and the improvement of atmospheric oxidation
430 capacity (Chen et al., 2020a; Feng et al., 2020). Therefore, more control measures should focus on weakening the
431 atmosphere oxidation capacity, such as reduction of O₃ formation, to reduce the formation of secondary pollutants
432 which are now identified as the most critical drivers of pollution. Considering those factors, it is also important to
433 promote the mitigation of *both* PM_{2.5} and O₃.

434 **4. Conclusion**

435 The intensive real-time measurement campaigns about PM_{2.5} chemical components were conducted in Xi'an,
436 Shijiazhuang, and Beijing during the wintertime respectively. Chemical compositions of PM_{2.5} in the three cities were
437 all dominated by OA (26.9–34.2%) and NO₃⁻ (23.6–26.5%). Six sources of PM_{2.5} in Xi'an and Shijiazhuang were
438 resolved by HERM and their contributions were similar, with a descending order of secondary nitrate plus sulfate
439 (32.2–37.6%), biomass burning (24.4–24.6 %), coal combustion (15.1–16.0%), vehicle emission (12.2–12.5 %),
440 industrial emission (5.5–7.7%) and fugitive dust (4.4–7.8%). However, the secondary nitrate (29.0%) and the
441 secondary sulfate (23.0%) were separately resolved and relatively more important in Beijing. In addition, the
442 contribution of firework (7.9%) to PM_{2.5} was found during the Chinese Spring Festival.

443 The possible formation mechanism of secondary nitrate plus sulfate in three pilot cities was explored. The results
444 showed that secondary aerosols were generated by both photochemical oxidation and aqueous-phase reaction.
445 Meanwhile, the formation rate of secondary aerosols in Beijing was higher than that in Xi'an and Shijiazhuang.
446 Furthermore, the eight pollution episodes within the sampling periods were categorized three types and characterized
447 respectively. The dominant chemical compositions of PM_{2.5} were OA (26–40%) and NO₃⁻ (23–32%) during all
448 pollution episodes. Furthermore, secondary nitrate plus sulfate and biomass burning were two major drivers of the
449 pollution.



450 The dominant chemical components of $PM_{2.5}$ in pilot cities have changed from OA and SO_4^{2-} to OA and NO_3^- under
451 the implementation of a clean air plan in past decades. This indicates that reduction of precursors including NO_2 and
452 VOCs should be a key task in the future. In addition, the contribution of biomass burning increased, especially in
453 Xi'an. This indicates that clean energy for heating activities in rural areas in northwest China is still insufficient.
454 Furthermore, to weaken the atmosphere oxidation capacity for reducing the contribution of secondary nitrate plus
455 sulfate, it is necessary to promote the collaborative control on ozone and particulate matter.

456 *Data availability.* Data used to support the findings in this study are archived at the Institute of Earth Environment,
457 Chinese Academy of Sciences, and are publicly available at <https://doi.org/10.5281/zenodo.7336744>.

458 *Competing interest.* The authors declare that they have no conflict of interest.

459 *Author contributions.* QW, YH, JC designed the campaigns. WR and YZ conducted the field measurements. YZ, JT,
460 HL, LQ and TC performed data analysis and interpretation. MM, KRD, JGS and ASHP were involved supervision
461 and review. YZ wrote the paper with contributions from all co-authors.

462 *Acknowledgments.* The authors are grateful to the staff from Guanzhong Plain, Eco-environmental Change and
463 Comprehensive Treatment, National Observation and Research Station; Tower Branch of Institute of Atmospheric
464 Physics, Chinese Academy Sciences; and Hebei Sailhero Environmental Protection High-tech Co., Ltd. for their
465 assistance with field sampling.

466 *Financial support.* This work was financially supported by the Sino-Swiss Cooperation on Air Pollution for Better
467 Air (7F-09802.01.02) from the Swiss Agency for Development and Cooperation (SDC), the National Key R&D
468 Program of China (2022YFF0802501), and the Youth Innovation Promotion Association of the Chinese Academy of
469 Sciences (2019402). Natural Science Basic Research Program of Shaanxi (2022JQ-267)

470



471 **References:**

- 472 Adachi, K. and Tainosho, Y.: Characterization of heavy metal particles embedded in tire dust, *Environ. Int.*, 30, 1009–
473 1017, <https://doi.org/10.1016/j.envint.2004.04.004>, 2004.
- 474 Ålander, T., Antikainen, E., Raunemaa, T., Elonen, E., Rautiola, A., and Torkkell, K.: Particle emissions from a small
475 Two-Stroke engine: Effects of fuel, lubricating oil, and exhaust aftertreatment on particle characteristics, *Aerosol*
476 *Sci. Technol.*, 39, 151–161, <https://doi.org/10.1080/027868290910224>, 2005.
- 477 Cao, J. J. and Cui, L.: Current status, characteristics and causes of particulate air pollution in the Fenwei Plain, China:
478 A Review, *J. Geophys. Res-Atmos.*, 126, <https://doi.org/10.1029/2020JD034472>, 2021.
- 479 Chan, C. K. and Yao, X.: Air pollution in mega cities in China, *Atmos. Environ.*, 42, 1–42,
480 <https://doi.org/10.1016/j.atmosenv.2007.09.003>, 2008.
- 481 Chen, L.-W. A. and Cao, J. J.: PM_{2.5} source apportionment using a hybrid environmental receptor model, *Environ.*
482 *Sci. Technol.*, 52, 6357–6369, <https://doi.org/10.1021/acs.est.8b00131>, 2018.
- 483 Chen, Q., Hua, X., Li, J. W., Chang, T., and Wang, Y.: Diurnal evolutions and sources of water-soluble chromophoric
484 aerosols over Xi'an during haze event, in Northwest China, *Sci. Total Environ.*, 786, 147412,
485 <https://doi.org/10.1016/j.scitotenv.2021.147412>, 2021.
- 486 Chen, S., Wang, H., Lu, K., Zeng, L., Hu, M., and Zhang, Y.: The trend of surface ozone in Beijing from 2013 to
487 2019: Indications of the persisting strong atmospheric oxidation capacity, *Atmos. Environ.*, 242, 117801,
488 <https://doi.org/10.1016/j.atmosenv.2020.117801>, 2020a.
- 489 Chen, Z., Chen, D., Zhao, C., Kwan, M., Cai, J., Zhuang, Y., Zhao, B., Wang, X., Chen, B., Yang, J., Li, R., He, B.,
490 Gao, B., Wang, K., and Xu, B.: Influence of meteorological conditions on PM_{2.5} concentrations across China: A
491 review of methodology and mechanism, *Environ. Int.*, 139, 105558,
492 <https://doi.org/10.1016/j.envint.2020.105558>, 2020b.
- 493 Chow, J. C., Lowenthal, D. H., Chen, L.-W. A., Wang, X., and Watson, J. G.: Mass reconstruction methods for PM_{2.5}:
494 a review, *Air Qual. Atmos. Health*, 8, 243–263, <https://doi.org/10.1007/s11869-015-0338-3>, 2015.
- 495 Dai, Q., Liu, B., Bi, X., Wu, J., Liang, D., Zhang, Y., Feng, Y., and Hopke, P. K.: Dispersion normalized PMF provides
496 insights into the significant changes in source contributions to PM_{2.5} after the COVID-19 outbreak, *Environ. Sci.*
497 *Technol.*, 54, 9917–9927, <https://doi.org/10.1021/acs.est.0c02776>, 2020.
- 498 DeCarlo, P. F., Ulbrich, I. M., Crouse, J., de Foy, B., Dunlea, E. J., Aiken, A. C., Knapp, D., Weinheimer, A. J.,
499 Campos, T., Wennberg, P. O., and Jimenez, J. L.: Investigation of the sources and processing of organic aerosol
500 over the Central Mexican Plateau from aircraft measurements during MILAGRO, *Atmos. Chem. Phys.*, 10,
501 5257–5280, <https://doi.org/10.5194/acp-10-5257-2010>, 2010.
- 502 Drinovec, L., Močnik, G., Zotter, P., Prévôt, A. S. H., Ruckstuhl, C., Coz, E., Rupakheti, M., Sciare, J., Müller, T.,
503 Wiedensohler, A., and Hansen, A. D. A.: The “dual-spo” Aethalometer: an improved measurement of aerosol
504 black carbon with real-time loading compensation, *Atmos. Meas. Tech.*, 8, 1965–1979,
505 <https://doi.org/10.5194/amt-8-1965-2015>, 2015.



- 506 Duan, J. and Tan, J.: Atmospheric heavy metals and Arsenic in China: Situation, sources and control policies, *Atmos.*
507 *Environ.*, 74, 93–101, <https://doi.org/10.1016/j.atmosenv.2013.03.031>, 2013.
- 508 Elser, M., Huang, R.-J., Wolf, R., Slowik, J. G., Wang, Q.-Y., Canonaco, F., Li, G. H., Bozzetti, C., Daellenbach, K.
509 R., Huang, Y., Zhang, R.-J., Li, Z.-Q., Cao, J. J., Baltensperger, U., El-Haddad, I., and Prévôt, A. S. H.: New
510 insights into PM_{2.5} chemical composition and sources in two major cities in China during extreme haze events
511 using aerosol mass spectrometry, *Aerosols/Field Measurements/Troposphere/Chemistry (chemical composition
512 and reactions)*, <https://doi.org/10.5194/acpd-15-30127-2015>, 2015.
- 513 Ervens, B., Turpin, B. J., and Weber, R. J.: Secondary organic aerosol formation in cloud droplets and aqueous
514 particles (aqSOA): a review of laboratory, field and model studies, *Atmos. Chem. Phys.*, 11, 11069–11102,
515 <https://doi.org/10.5194/acp-11-11069-2011>, 2011.
- 516 Feng, T., Bei, N., Zhao, S., Wu, J. rui, Li, X., Zhang, T., Cao, J., Zhou, W., and Li, G.: Wintertime nitrate formation
517 during haze days in the Guanzhong basin, China: A case study, *Environ. Pollut.*, 243, 1057–1067,
518 <https://doi.org/10.1016/j.envpol.2018.09.069>, 2018.
- 519 Feng, T., Zhao, S., Zhang, X., Wang, Q., Liu, L., Li, G., and Tie, X.: Increasing wintertime ozone levels and secondary
520 aerosol formation in the Guanzhong basin, central China, *Sci. Total Environ.*, 12, 2020.
- 521 Feng, X., Zhang, X., He, C., and Wang, J.: Contributions of traffic and industrial emission reductions to the air quality
522 improvement after the lockdown of Wuhan and neighboring Cities due to COVID-19, *Toxics*, 9, 358,
523 <https://doi.org/10.3390/toxics9120358>, 2021.
- 524 Fermo, P., Artifianno, B., De Gennaro, G., Pantaleo, A. M., Parente, A., Battaglia, F., Colicino, E., Di Tanna, G.,
525 Goncalves da Silva Junior, A., Pereira, I. G., Garcia, G. S., Garcia Goncalves, L. M., Comite, V., and Miani, A.:
526 Improving indoor air quality through an air purifier able to reduce aerosol particulate matter (PM) and volatile
527 organic compounds (VOCs): Experimental results, *Environ. Pollut.*, 197, 111131,
528 <https://doi.org/10.1016/j.envres.2021.111131>, 2021.
- 529 Fontaras, G., Martini, G., Manfredi, U., Marotta, A., Krasenbrink, A., Maffioletti, F., Terenghi, R., and Colombo, M.:
530 Assessment of on-road emissions of four Euro V diesel and CNG waste collection trucks for supporting air-
531 quality improvement initiatives in the city of Milan, *Sci. Total Environ.*, 426, 65–72,
532 <https://doi.org/10.1016/j.scitotenv.2012.03.038>, 2012.
- 533 Fountoukis, C. and Nenes, A.: ISORROPIA II: a computationally efficient thermodynamic equilibrium model for
534 $K^+ - Ca^{2+} - Mg^{2+} - NH_4^+ - Na^+ - SO_4^{2-} - NO_3^- - Cl^- - H_2O$ aerosols, *Atmos. Chem. Phys.*, 7, 4639–4659,
535 <https://doi.org/10.5194/acp-7-4639-2007>, 2007.
- 536 Furger, M., Rai, P., Slowik, J. G., Cao, J., Visser, S., Baltensperger, U., and Prévôt, A. S. H.: Automated alternating
537 sampling of PM₁₀ and PM_{2.5} with an online XRF spectrometer, *Atmospheric Environment: X*, 5, 100065,
538 <https://doi.org/10.1016/j.aeaoa.2020.100065>, 2020.
- 539
- 540 Gu, B., Zhang, L., Van Dingenen, R., Vieno, M., Van Grinsven, H. J., Zhang, X., Zhang, S., Chen, Y., Wang, S., Ren,
541 C., Rao, S., Holland, M., Winiwarter, W., Chen, D., Xu, J., and Sutton, M. A.: Abating ammonia is more cost-
542 effective than nitrogen oxides for mitigating PM_{2.5} air pollution, *Science*, 374, 758–762,



- 543 <https://doi.org/10.1126/science.abf8623>, 2021.
- 544 Guo, Y., Lin, C., Li, J., Wei, L., Yang, Y., Yang, Q., Li, D., Wang, H., and Shen, J.: Persistent pollution episodes,
545 transport pathways, and potential sources of air pollution during the heating season of 2016–2017 in Lanzhou,
546 China, *Environ. Monit. Assess.*, 193, 852, <https://doi.org/10.1007/s10661-021-09597-8>, 2021.
- 547 He, J., Zhao, M., Zhang, B., Wang, P., Zhang, D., Wang, M., Liu, B., Li, N., Yu, K., Zhang, Y., Zhou, T., and Jing, B.:
548 The impact of steel emissions on air quality and pollution control strategy in Caofeidian, North China, *Atmos.*
549 *Pollut. Res.*, 11, 1238–1247, <https://doi.org/10.1016/j.apr.2020.04.012>, 2020.
- 550 He, K., Huo, H., and Zhang, Q.: Urban air pollution in China: Current status, characteristics, and progress, *Annu.*
551 *Rev. Energy. Environ.*, 27, 397–431, <https://doi.org/10.1146/annurev.energy.27.122001.083421>, 2002.
- 552 Hu, W. wei, Campuzano-Jost, P., Day, D. A., Croteau, P., Canagaratna, M. R., Jayne, J. T., Worsnop, D. R., and
553 Jimenez, J. L.: Evaluation of the new capture vapourizer for aerosol mass spectrometers (AMS) through
554 laboratory studies of inorganic species, *Atmos. Meas. Tech.*, 10, 2897–2921, <https://doi.org/10.5194/amt-10-2897-2017>, 2017.
- 556 Huang, R.-J., He, Y., Duan, J., Li, Y., Chen, Q., Zheng, Y., Chen, Y., Hu, W., Lin, C., Ni, H., Dai, W., Cao, J., Wu, Y.,
557 Zhang, R., Xu, W., Ovadnevaite, J., Ceburnis, D., Hoffmann, T., and O’Dowd, C. D.: Contrasting sources and
558 processes of particulate species in haze days with low and high relative humidity in wintertime Beijing, *Atmos.*
559 *Chem. Phys.*, 20, 9101–9114, <https://doi.org/10.5194/acp-20-9101-2020>, 2020.
- 560 Huang, R.-J., Zhang, Y., Bozzetti, C., Ho, K.-F., Cao, J.-J., Han, Y., Daellenbach, K. R., Slowik, J. G., Platt, S. M.,
561 Canonaco, F., Zotter, P., Wolf, R., Pieber, S. M., Bruns, E. A., Crippa, M., Ciarelli, G., Piazzalunga, A.,
562 Schwikowski, M., Abbaszade, G., Schnelle-Kreis, J., Zimmermann, R., An, Z., Szidat, S., Baltensperger, U.,
563 Haddad, I. E., and Prévôt, A. S. H.: High secondary aerosol contribution to particulate pollution during haze
564 events in China, *Nature*, 514, 218–222, <https://doi.org/10.1038/nature13774>, 2014.
- 565 Huang, X., Liu, Z., Liu, J., Hu, B., Wen, T., Tang, G., Zhang, J., Wu, F. kun, Ji, D., Wang, L., and Wang, Y.: Chemical
566 characterization and source identification of PM_{2.5} at multiple sites in the Beijing–Tianjin–Hebei region, China,
567 *Atmos. Chem. Phys.*, 17, 12941–12962, <https://doi.org/10.5194/acp-17-12941-2017>, 2017.
- 568 Huang, R.-J., Wang, Y., Cao, J., Lin, C., Duan, J., Chen, Q., Li, Y., Gu, Y., Yan, J., Xu, W., Fröhlich, R., Canonaco,
569 F., Bozzetti, C., Ovadnevaite, J., Ceburnis, D., Canagaratna, M. R., Jayne, J., Worsnop, D. R., El-Haddad, I.,
570 Prévôt, A. S. H., and O’Dowd, C. D.: Primary emissions versus secondary formation of fine particulate matter
571 in the most polluted city (Shijiazhuang) in North China, *Atmos. Chem. Phys.*, 19, 2283–2298,
572 <https://doi.org/10.5194/acp-19-2283-2019>, 2019.
- 573
- 574 Huang, X., Zhang, J., Luo, B., Luo, J., Zhang, W., and Rao, Z.: Characterization of oxalic acid-containing particles
575 in summer and winter seasons in Chengdu, China, *Atmos. Environ.*, 198, 133–141,
576 <https://doi.org/10.1016/j.atmosenv.2018.10.050>, 2019.
- 577 Jin, T. sheng, Gao, J. jia, Fu, L. xin, Ai, Y., and Xu, X. H.: An evaluation of improvements in the air quality of Beijing
578 arising from the use of new vehicle emission standards, *Environ. Monit. Assess.*, 184, 2151–2159,
579 <https://doi.org/10.1007/s10661-011-2106-7>, 2012.



- 580 Khan, M. A. H., Ashfold, M. J., Nickless, G., Martin, D., Watson, L. A., Hamer, P. D., Wayne, R. P., Canosa-Mas, C.
581 E., and Shallcross, D. E.: Night-time NO₃ and OH radical concentrations in the United Kingdom inferred from
582 hydrocarbon measurements, *Atmos. Sci. Lett.*, 9, 140–146, <https://doi.org/10.1002/asl.175>, 2008.
- 583 Kuniyal, J. C. and Guleria, R. P.: The current state of aerosol-radiation interactions: A mini review, *J. Aerosol Sci.*,
584 130, 45–54, <https://doi.org/10.1016/j.jaerosci.2018.12.010>, 2019.
- 585 Kuo, C.-Y., Cheng, F.-C., Chang, S.-Y., Lin, C.-Y., Chou, C. C. K., Chou, C.-H., and Lin, Y.-R.: Analysis of the major
586 factors affecting the visibility degradation in two stations, *J. Air Waste Manage.*, 63, 433–441,
587 <https://doi.org/10.1080/10962247.2012.762813>, 2013.
- 588 Ledoux, F., Kfoury, A., Delmaire, G., Roussel, G., El Zein, A., and Courcot, D.: Contributions of local and regional
589 anthropogenic sources of metals in PM_{2.5} at an urban site in northern France, *Chemosphere*, 181, 713–724,
590 <https://doi.org/10.1016/j.chemosphere.2017.04.128>, 2017.
- 591 Lewis, C. W., Norris, G. A., Conner, T. L., and Henry, R. C.: Source apportionment of Phoenix PM_{2.5} aerosol with
592 the Unmix receptor model, *J. Air Waste Manage.*, 53, 325–338,
593 <https://doi.org/10.1080/10473289.2003.10466155>, 2003.
- 594 Li, J., Du, H., Wang, Z., Sun, Y., Yang, W., He, J., Tang, X., and Fu, P.: Rapid formation of a severe regional winter
595 haze episode over a mega-city cluster on the North China Plain, *Environ. Pollut.*, 223, 605–615,
596 <https://doi.org/10.1016/j.envpol.2017.01.063>, 2017a.
- 597
- 598 Li, J., Gao, W., Cao, L., Xiao, Y., Zhang, Y., Zhao, S., Liu, Z., Liu, Z., Tang, G., Ji, D., Hu, B., Song, T., He, L., Hu,
599 M., and Wang, Y.: Significant changes in autumn and winter aerosol composition and sources in Beijing from
600 2012 to 2018: Effects of clean air actions, *Environ. Pollut.*, 268, 115855,
601 <https://doi.org/10.1016/j.envpol.2020.115855>, 2021a.
- 602 Li, K., Zhang, X., Zhao, B., Bloss, W. J., Lin, C., White, S., Yu, H., Chen, L., Geng, C., Yang, W., Azzi, M., George,
603 C., and Bai, Z.: Suppression of anthropogenic secondary organic aerosol formation by isoprene, *npj Clim. Atmos.*
604 *Sci.*, 5, 12, <https://doi.org/10.1038/s41612-022-00233-x>, 2022.
- 605 Li, L., Tan, Q., Zhang, Y., Feng, M., Qu, Y., An, J., and Liu, X.: Characteristics and source apportionment of PM_{2.5}
606 during persistent extreme haze events in Chengdu, southwest China, *Environ. Pollut.*, 230, 718–729,
607 <https://doi.org/10.1016/j.envpol.2017.07.029>, 2017b.
- 608 Li, W., Shao, L. yi, Wang, W., Li, H., Wang, X., Li, Y., Li, W., Jones, T., and Zhang, D.: Air quality improvement in
609 response to intensified control strategies in Beijing during 2013–2019, *Sci. Total Environ.*, 744, 140776,
610 <https://doi.org/10.1016/j.scitotenv.2020.140776>, 2020.
- 611 Li, X., Bei, N., Tie, X., Wu, J., Liu, S., Wang, Q., Liu, L., Wang, R., and Li, G.: Local and transboundary transport
612 contributions to the wintertime particulate pollution in the Guanzhong Basin (GZB), China: A case study, *Sci.*
613 *Total Environ.*, 797, 148876, <https://doi.org/10.1016/j.scitotenv.2021.148876>, 2021b.
- 614 Li, Y., Sun, Y., Zhang, Q., Li, X., Li, M., Zhou, Z., and Chan, C. K.: Real-time chemical characterization of
615 atmospheric particulate matter in China: A review, *Atmos. Environ.*, 158, 270–304,



- 616 <https://doi.org/10.1016/j.atmosenv.2017.02.027>, 2017c.
- 617 Liu, J., Chen, Y., Chao, S., Cao, H., Zhang, A., Yang, Y.: Emission control priority of PM_{2.5}-bound heavy metals in
618 different seasons: A comprehensive analysis from health risk perspective, *Sci. Total Environ.*, 644, 20-30.
619 <https://doi.org/10.1016/j.scitotenv.2018.06.226>, 2018a.
- 620 Liu, B., Cheng, Y., Zhou, M., Liang, D., Dai, Q., Wang, L., Jin, W., Zhang, L., Ren, Y., Zhou, J., Dai, C., Xu, J.,
621 Wang, J., Feng, Y., and Zhang, Y.: Effectiveness evaluation of temporary emission control action in 2016 in
622 winter in Shijiazhuang, China, *Atmos. Chem. Phys.*, 18, 7019–7039, <https://doi.org/10.5194/acp-18-7019-2018>,
623 2018b.
- 624 Liu, J., Chu, B., Jia, Y., Cao, Q., Zhang, H., Chen, T., Ma, Q., Ma, J., Wang, Y., Zhang, P., and He, H.: Dramatic
625 decrease of secondary organic aerosol formation potential in Beijing: Important contribution from reduction of
626 coal combustion emission, *Sci. Total Environ.*, 832, 155045, <https://doi.org/10.1016/j.scitotenv.2022.155045>,
627 2022.
- 628 Liu, Y., Zheng, M., Yu, M., Cai, X., Du, H., Li, J., Zhou, T., Yan, C., Wang, X., Shi, Z., Harrison, R. M., Zhang, Q.,
629 and He, K.: High-time-resolution source apportionment of PM_{2.5} in Beijing with multiple models, *Atmos. Chem.*
630 *Phys.*, 19, 6595–6609, <https://doi.org/10.5194/acp-19-6595-2019>, 2019.
- 631 Liu, Z., Wang, Y., Hu, B., Ji, D., Zhang, J., Wu, F., Wan, X., and Wang, Y.: Source appointment of fine particle number
632 and volume concentration during severe haze pollution in Beijing in January 2013, *Environ. Sci. Pollut. Res.*,
633 23, 6845–6860, <https://doi.org/10.1007/s11356-015-5868-6>, 2016.
- 634
- 635 Long, X., Li, N., Tie, X., Cao, J., Zhao, S., Huang, R., Zhao, M., Li, G., and Feng, T.: Urban dust in the Guanzhong
636 Basin of China, part I: A regional distribution of dust sources retrieved using satellite data, *Sci. Total Environ.*,
637 541, 1603–1613, <https://doi.org/10.1016/j.scitotenv.2015.10.063>, 2016.
- 638 Lu, J., Ge, P., Zhao, Y.: Recent development of effect mechanism of alloying elements in titanium alloy design, *Rare*
639 *Metal Mat. Eng.*, 43, 775-779. [https://doi.org/10.1016/S1875-5372\(14\)60082-5](https://doi.org/10.1016/S1875-5372(14)60082-5), 2014.
- 640 Lu, W., Tian, Q., Xu, R., Qiu, L., Fan, Z., Wang, S., Liu, T., Huang, J., Li, Y., Wang, Y., Shi, C., Liu, Y., and Zhou,
641 Y.: Ambient air pollution and hospitalization for chronic obstructive pulmonary disease: Benefits from Three-
642 Year Action Plan, *Ecotoxicol. Environ. Saf.*, 228, 113034, <https://doi.org/10.1016/j.ecoenv.2021.113034>, 2021.
- 643 Lv, B., Zhang, B., and Bai, Y.: A systematic analysis of PM_{2.5} in Beijing and its sources from 2000 to 2012, *Atmos.*
644 *Environ.*, 124, 98–108, <https://doi.org/10.1016/j.atmosenv.2015.09.031>, 2016.
- 645 Lv, L., Chen, Y., Han, Y., Cui, M., Wei, P., Zheng, M., and Hu, J.: High-time-resolution PM_{2.5} source apportionment
646 based on multi-model with organic tracers in Beijing during haze episodes, *Sci. Total Environ.*, 772, 144766,
647 <https://doi.org/10.1016/j.scitotenv.2020.144766>, 2021.
- 648 Ma, Y., Huang, Y., Wu, J., E, J., Zhang, B., Han, D., and Ong, H. C.: A review of atmospheric fine particulate matters:
649 chemical composition, source identification and their variations in Beijing, *Energ. Source. Part A*, 44, 4783–
650 4807, <https://doi.org/10.1080/15567036.2022.2075991>, 2022.



- 651 Meng, H., Shen, Y., Fang, Y., and Zhu, Y.: Impact of the ‘Coal-to-Natural Gas’ Policy on Criteria Air Pollutants in
652 Northern China, *Atmosphere*, 13, 945, <https://doi.org/10.3390/atmos13060945>, 2022.
- 653 Meng, J., Wang, G., Li, J., Cheng, C., Ren, Y., Huang, Y., Cheng, Y., Cao, J., and Zhang, T.: Seasonal characteristics
654 of oxalic acid and related SOA in the free troposphere of Mt. Hua, central China: Implications for sources and
655 formation mechanisms, *Sci. Total Environ.*, 493, 1088–1097, <https://doi.org/10.1016/j.scitotenv.2014.04.086>,
656 2014.
- 657 Ng, N. L., Herndon, S. C., Trimborn, A., Canagaratna, M. R., Croteau, P. L., Onasch, T. B., Sueper, D., Worsnop, D.
658 R., Zhang, Q., Sun, Y. L., and Jayne, J. T.: An Aerosol Chemical Speciation Monitor (ACSM) for Routine
659 Monitoring of the Composition and Mass Concentrations of Ambient Aerosol, *Aerosol Sci. Technol.*, 45, 780–
660 794, <https://doi.org/10.1080/02786826.2011.560211>, 2011.
- 661 Ni, H., Tian, J., Wang, X., Wang, Q., Han, Y., Cao, J., Long, X., Chen, L.-W. A., Chow, J. C., Watson, J. G., Huang,
662 R.-J., and Dusek, U.: PM_{2.5} emissions and source profiles from open burning of crop residues, *Atmos. Environ.*,
663 169, 229–237, <https://doi.org/10.1016/j.atmosenv.2017.08.063>, 2017.
- 664 Ouyang, J., Song, L.-J., Ma, L.-L., Luo, M., Dai, X.-X., Zhang, J.-T., and Xu, D.-D.: Quantification of secondary
665 particle loading during a heavy air pollution event in Beijing: A simplified method based on coal emission
666 indicators, *Atmos. Environ.*, 215, 116896, <https://doi.org/10.1016/j.atmosenv.2019.116896>, 2019.
- 667 Pant, P. and Harrison, R.M.: Estimation of the contribution of road traffic emissions to particulate matter
668 concentrations from field measurements: A review, *Atmos. Environ.*, 77, 78–97.
669 <https://doi.org/10.1016/j.atmosenv.2013.04.028>, 2013.
- 670 Pang, N., Gao, J., Zhu, G., Hui, L., Zhao, P., Xu, Z., Tang, W., and Chai, F.: Impact of clean air action on the PM_{2.5}
671 pollution in Beijing, China: Insights gained from two heating seasons measurements, *Chemosphere*, 263,
672 127991, <https://doi.org/10.1016/j.chemosphere.2020.127991>, 2021.
- 673 Pöschl, U.: Atmospheric Aerosols: Composition, Transformation, Climate and Health Effects, *Angew. Chem. Int. Ed.*,
674 44, 7520–7540, <https://doi.org/10.1002/anie.200501122>, 2005.
- 675 Pui, D. Y. H., Chen, S.-C., and Zuo, Z.: PM_{2.5} in China: Measurements, sources, visibility and health effects, and
676 mitigation, *Particuology*, 13, 1–26, <https://doi.org/10.1016/j.partic.2013.11.001>, 2014.
- 677 Rai, P., Furger, M., Slowik, J. G., Canonaco, F., Fröhlich, R., Hüglin, C., Minguillón, M. C., Pettersson, K.,
678 Baltensperger, U., and Prévôt, A. S. H.: Source apportionment of highly time-resolved elements during a
679 firework episode from a rural freeway site in Switzerland, *Atmos. Chem. Phys.*, 20, 1657–1674,
680 <https://doi.org/10.5194/acp-20-1657-2020>, 2020.
- 681 Ren, Y.: Chemical components and source identification of PM_{2.5} in non-heating season in Beijing: The influences
682 of biomass burning and dust, *Atmos. Res.*, 8, 2021.
- 683 Shen, G.: Changes from traditional solid fuels to clean household energies – Opportunities in emission reduction of
684 primary PM_{2.5} from residential cookstoves in China, *Biomass Bioenerg.*, 86, 28–35,
685 <https://doi.org/10.1016/j.biombioe.2016.01.004>, 2016.



- 686 Shen, W.-T., Yu, X., Zhong, S.-B., and Ge, H.-R.: Population Health Effects of Air Pollution: Fresh Evidence From
687 China Health and Retirement Longitudinal Survey, *Front. Public Health*, 9, 779552,
688 <https://doi.org/10.3389/fpubh.2021.779552>, 2021.
- 689 Shen, Z., Sun, J., Cao, J., Zhang, L., Zhang, Q., Lei, Y., Gao, J., Huang, R.-J., Liu, S., Huang, Y., Zhu, C., Xu, H.,
690 Zheng, C., Liu, P., and Xue, Z.: Chemical profiles of urban fugitive dust PM_{2.5} samples in Northern Chinese
691 cities, *Sci. Total Environ.*, 569–570, 619–626, <https://doi.org/10.1016/j.scitotenv.2016.06.156>, 2016.
- 692 Simka, H., Shankar, S., Duran, C., and Haverty, M.: Fundamentals of Cu/Barrier-Layer Adhesion in Microelectronic
693 Processing, *MRS Proc.*, 863, B9.2, <https://doi.org/10.1557/PROC-863-B9.2>, 2005.
- 694 Tao, J., Zhang, L., Cao, J., and Zhang, R.: A review of current knowledge concerning PM_{2.5} chemical composition,
695 aerosol optical properties and their relationships across China, *Atmos. Chem. Phys.*, 17, 9485–9518,
696 <https://doi.org/10.5194/acp-17-9485-2017>, 2017. Tao, J., Zhang, L., Zhang, Z., Huang, R., Wu, Y., Zhang, R.,
697 Cao, J., and Zhang, Y.: Control of PM_{2.5} in Guangzhou during the 16th Asian Games period: Implication for
698 hazy weather prevention, *Sci. Total Environ.*, 508, 57–66, <https://doi.org/10.1016/j.scitotenv.2014.11.074>, 2015.
- 699 Tao, Y., Ye, X., Ma, Z., Xie, Y., Wang, R., Chen, J., Yang, X., and Jiang, S.: Insights into different nitrate formation
700 mechanisms from seasonal variations of secondary inorganic aerosols in Shanghai, *Atmos. Environ.*, 145, 1–9,
701 <https://doi.org/10.1016/j.atmosenv.2016.09.012>, 2016.
- 702 Thorpe, A. and Harrison, R. M.: Sources and properties of non-exhaust particulate matter from road traffic: A review,
703 *Sci. Total Environ.*, 400, 270–282, <https://doi.org/10.1016/j.scitotenv.2008.06.007>, 2008.
- 704 Tian, H. Z., Lu, L., Hao, J. M., Gao, J. J., Cheng, K., Liu, K. Y., Qiu, P. P., and Zhu, C. Y.: A Review of key hazardous
705 trace elements in Chinese coals: Abundance, occurrence, behavior during coal combustion and their
706 environmental impacts, *Energ. Fuel.*, 27, 601–614, <https://doi.org/10.1021/ef3017305>, 2013.
- 707 Tian, J., Wang, Q., Zhang, Y., Yan, M., Liu, H., Zhang, N., Ran, W., and Cao, J.: Impacts of primary emissions and
708 secondary aerosol formation on air pollution in an urban area of China during the COVID-19 lockdown, *Environ.*
709 *Int.*, 150, 106426, <https://doi.org/10.1016/j.envint.2021.106426>, 2021.
- 710 Tian, J., Wang, Q., Liu, H., Ma, Y., Liu, S., Zhang, Y., Ran, W., Han, Y., and Cao, J.: Measurement report: The
711 importance of biomass burning in light extinction and direct radiative effect of urban aerosol during the COVID-
712 19 lockdown in Xi'an, China, *Atmos. Chem. Phys.*, 22, 8369–8384, <https://doi.org/10.5194/acp-22-8369-2022>,
713 2022.
- 714 Tian, Y. Z., Wang, J., Peng, X., Shi, G. L., and Feng, Y. C.: Estimation of the direct and indirect impacts of fireworks
715 on the physicochemical characteristics of atmospheric PM₁₀ and PM_{2.5}, *Atmos. Chem. Phys.*, 14, 9469–9479,
716 <https://doi.org/10.5194/acp-14-9469-2014>, 2014.
- 717 Vu, T. V., Shi, Z., Cheng, J., Zhang, Q., He, K., Wang, S., and Harrison, R. M.: Assessing the impact of clean air
718 action on air quality trends in Beijing using a machine learning technique, *Atmos. Chem. Phys.*, 19, 11303–
719 11314, <https://doi.org/10.5194/acp-19-11303-2019>, 2019.
- 720 Wang, C., Li, X., Zhang, T., Tang, A., Cui, M., Liu, X., Ma, X., Zhang, Y., Liu, X., and Zheng, M.: Developing
721 Nitrogen Isotopic Source Profiles of Atmospheric Ammonia for Source Apportionment of Ammonia in Urban



- 722 Beijing, *Front. Environ. Sci.*, 10, 903013, <https://doi.org/10.3389/fenvs.2022.903013>, 2022a.
- 723 Wang, F., Yu, H., Wang, Z., Liang, W., Shi, G., Gao, J., Li, M., and Feng, Y.: Review of online source apportionment
724 research based on observation for ambient particulate matter, *Sci. Total Environ.*, 762, 144095,
725 <https://doi.org/10.1016/j.scitotenv.2020.144095>, 2021a.
- 726 Wang, H. and Zhao, L.: A joint prevention and control mechanism for air pollution in the Beijing-Tianjin-Hebei
727 region in china based on long-term and massive data mining of pollutant concentration, *Atmos. Environ.*, 174,
728 25–42, <https://doi.org/10.1016/j.atmosenv.2017.11.027>, 2018.
- 729 Wang, J., Zhao, B., Wang, S., Yang, F., Xing, J., Morawska, L., Ding, A., Kulmala, M., Kerminen, V.-M., Kujansuu,
730 J., Wang, Z., Ding, D., Zhang, X., Wang, H., Tian, M., Petäjä, T., Jiang, J., and Hao, J.: Particulate matter
731 pollution over China and the effects of control policies, *Sci. Total Environ.*, 584–585, 426–447,
732 <https://doi.org/10.1016/j.scitotenv.2017.01.027>, 2017.
- 733 Wang, L., Wang, X., Gu, R., Wang, H., Yao, L., Wen, L., Zhu, F., Wang, W., Xue, L., Yang, L., Lu, K., Chen, J., Wang,
734 T., Zhang, Y., and Wang, W.: Observations of fine particulate nitrated phenols in four sites in northern China:
735 concentrations, source apportionment, and secondary formation, *Atmos. Chem. Phys.*, 18, 4349–4359,
736 <https://doi.org/10.5194/acp-18-4349-2018>, 2018.
- 737 Wang, L. T., Wei, Z., Yang, J., Zhang, Y., Zhang, F. F., Su, J., Meng, C. C., and Zhang, Q.: The 2013 severe haze over
738 southern Hebei, China: model evaluation, source apportionment, and policy implications, *Atmos. Chem. Phys.*,
739 14, 3151–3173, <https://doi.org/10.5194/acp-14-3151-2014>, 2014.
- 740 Wang, M., Tian, P., Wang, L., Yu, Z., Du, T., Chen, Q., Guan, X., Guo, Y., Zhang, M., Tang, C., Chang, Y., Shi, J.,
741 Liang, J., Cao, X., and Zhang, L.: High contribution of vehicle emissions to fine particulate pollutions in
742 Lanzhou, Northwest China based on high-resolution online data source appointment, *Sci. Total Environ.*, 798,
743 149310, <https://doi.org/10.1016/j.scitotenv.2021.149310>, 2021b.
- 744 Wang, P., Cao, J., Shen, Z., Han, Y., Lee, S., Huang, Y., Zhu, C., Wang, Q., Xu, H., and Huang, R.: Spatial and
745 seasonal variations of PM_{2.5} mass and species during 2010 in Xi'an, China, *Sci. Total Environ.*, 508, 477–487,
746 <https://doi.org/10.1016/j.scitotenv.2014.11.007>, 2015.
- 747 Wang, Q., Ye, J., Wang, Y., Zhang, T., Ran, W., Wu, Y., Tian, J., Li, L., Zhou, Y., Hang Ho, S. S., Dang, B., Zhang,
748 Q., Zhang, R., Chen, Y., Zhu, C., and Cao, J.: Wintertime Optical Properties of Primary and Secondary Brown
749 Carbon at a Regional Site in the North China Plain, *Environ. Sci. Technol.*, 53, 12389–12397,
750 <https://doi.org/10.1021/acs.est.9b03406>, 2019.
- 751 Wang, Y., Wang, Q., Ye, J., Yan, M., Qin, Q., Prévôt, A. S. H., and Cao, J.: A Review of Aerosol Chemical
752 Composition and Sources in Representative Regions of China during Wintertime, *Atmosphere*, 10, 277,
753 <https://doi.org/10.3390/atmos10050277>, 2019.
- 754 Wang, Y., Zhang, Q. Q., He, K., Zhang, Q., and Chai, L.: Sulfate-nitrate-ammonium aerosols over China: response
755 to 2000–2015 emission changes of sulfur dioxide, nitrogen oxides, and ammonia, *Atmos. Chem. Phys.*, 13,
756 2635–2652, <https://doi.org/10.5194/acp-13-2635-2013>, 2013.
- 757 Wang, Y., Yuan, Y., Wang, Q., Liu, C., Zhi, Q., and Cao, J.: Changes in air quality related to the control of coronavirus



- 758 in China: Implications for traffic and industrial emissions, *Sci. Total Environ.*, 731, 139133,
759 <https://doi.org/10.1016/j.scitotenv.2020.139133>, 2020a.
- 760 Wang, Y., Yu, M., Wang, Y., Tang, G., Song, T., Zhou, P., Liu, Z., Hu, B., Ji, D., Wang, L., Zhu, X., Yan, C., Ehn, M.,
761 Gao, W., Pan, Y., Xin, J., Sun, Y., Kerminen, V.-M., Kulmala, M., and Petäjä, T.: Rapid formation of intense
762 haze episodes via aerosol–boundary layer feedback in Beijing, *Atmos. Chem. Phys.*, 20, 45–53,
763 <https://doi.org/10.5194/acp-20-45-2020>, 2020b.
- 764 Wang, Y., Liu, C., Wang, Q., Qin, Q., Ren, H., and Cao, J.: Impacts of natural and socioeconomic factors on PM_{2.5}
765 from 2014 to 2017, *J. Environ. Manage.*, 284, 112071, <https://doi.org/10.1016/j.jenvman.2021.112071>, 2021c.
- 766 Wang, Z., Wang, R., Wang, J., Wang, Y., McPherson Donahue, N., Tang, R., Dong, Z., Li, X., Wang, L., Han, Y., and
767 Cao, J.: The seasonal variation, characteristics and secondary generation of PM_{2.5} in Xi'an, China, especially
768 during pollution events, *Environ. Res.*, 212, 113388, <https://doi.org/10.1016/j.envres.2022.113388>, 2022b.
- 769 Wei, F., Yang G., Jiang, D., Liu, Z., Sun, B.: Basic statistics and characteristics of background values of soil elements
770 in China. *Environ. Monit. in China (in Chinese)* 7, 1–6. <https://doi.org/10.19316/j.issn.1002-6002.1991.01.001>,
771 1991.
- 772 Wood, E. C., Canagaratna, M. R., Herndon, S. C., Onasch, T. B., Kolb, C. E., Worsnop, D. R., Kroll, J. H., Knighton,
773 W. B., Seila, R., Zavala, M., Molina, L. T., DeCarlo, P. F., Jimenez, J. L., Weinheimer, A. J., Knapp, D. J., Jobson,
774 B. T., Stutz, J., Kuster, W. C., and Williams, E. J.: Investigation of the correlation between odd oxygen and
775 secondary organic aerosol in Mexico City and Houston, *Atmos. Chem. Phys.*, 10, 8947–8968,
776 <https://doi.org/10.5194/acp-10-8947-2010>, 2010.
- 777 Xu, H. M., Cao, J. J., Ho, K. F., Ding, H., Han, Y. M., Wang, G. H., Chow, J. C., Watson, J. G., Khol, S. D., Qiang,
778 J., and Li, W. T.: Lead concentrations in fine particulate matter after the phasing out of leaded gasoline in Xi'an,
779 China, *Atmos. Environ.*, 46, 217–224, <https://doi.org/10.1016/j.atmosenv.2011.09.078>, 2012.
- 780 Xu, J., Liu, D., Wu, X., Vu, T. V., Zhang, Y., Fu, P., Sun, Y., Xu, W., Zheng, B., Harrison, R. M., and Shi, Z.: Source
781 apportionment of fine organic carbon at an urban site of Beijing using a chemical mass balance model, *Atmos.*
782 *Chem. Phys.*, 21, 2021.
- 783 Xu, P., Yang, Y., Zhang, J., Gao, W., Liu, Z., Hu, B., and Wang, Y.: Characterization and source identification of
784 submicron aerosol during serious haze pollution periods in Beijing, *J. of Environ. Sci.*, 112, 25–37,
785 <https://doi.org/10.1016/j.jes.2021.04.005>, 2022.
- 786 Xu, W., Croteau, P., Williams, L., Canagaratna, M., Onasch, T., Cross, E., Zhang, X., Robinson, W., Worsnop, D.,
787 and Jayne, J.: Laboratory characterization of an aerosol chemical speciation monitor with PM_{2.5} measurement
788 capability, *Aerosol Sci. Technol.*, 51, 69–83, <https://doi.org/10.1080/02786826.2016.1241859>, 2017.
- 789 Xue, J., Griffith, S. M., Yu, X., Lau, A. K. H., and Yu, J. Z.: Effect of nitrate and sulfate relative abundance in PM_{2.5}
790 on liquid water content explored through half-hourly observations of inorganic soluble aerosols at a polluted
791 receptor site, *Atmos. Environ.*, 99, 24–31, <https://doi.org/10.1016/j.atmosenv.2014.09.049>, 2014.
- 792 Yan, Y., Sun, Y. B., Weiss, D., Liang, L. J., and Chen, H. Y.: Polluted dust derived from long-range transport as a
793 major end member of urban aerosols and its implication of non-point pollution in northern China, *Sci. Total*



- 794 Environ., 506–507, 538–545, <https://doi.org/10.1016/j.scitotenv.2014.11.071>, 2015.
- 795 Yang, D., Li, Z., Yue, Z., Liu, J. X., Zhai, Z., Li, Z., Gao, M., Hu, A. L., Zhu, W. J., Ding, N., Li, Z., Guo, S., Wang,
796 X., Wang, L., and Wei, J.: Variations in sources, composition, and exposure risks of PM_{2.5} in both pre-heating
797 and heating seasons, *Aerosol Air Qual. Res.*, 22, 14, <https://doi.org/10.4209/aaqr.210333>, 2022a.
- 798 Yang, S., Yuan, B., Peng, Y., Huang, S., Chen, W., Hu, W., Pei, C., Zhou, J., Parrish, D. D., Wang, W., He, X., Cheng,
799 C., Li, X.-B., Yang, X., Song, Y., Wang, H., Qi, J., Wang, B., Wang, C., Wang, C., Wang, Z., Li, T., Zheng, E.,
800 Wang, S., Wu, C., Cai, M., Ye, C., Song, W., Cheng, P., Chen, D., Wang, X., Zhang, Z., Wang, X., Zheng, J.,
801 and Shao, M.: The formation and mitigation of nitrate pollution: comparison between urban and suburban
802 environments, *Atmos. Chem. Phys.*, 22, 4539–4556, <https://doi.org/10.5194/acp-22-4539-2022>, 2022b.
- 803 Yang, X. and Teng, F.: The air quality co-benefit of coal control strategy in China, *Resour. Conserv. Recy.*, 129, 373–
804 382, <https://doi.org/10.1016/j.resconrec.2016.08.011>, 2018.
- 805 Yang, X., Zheng, M., Liu, Y., Yan, C., Liu, J., Liu, J., and Cheng, Y.: Exploring sources and health risks of metals in
806 Beijing PM_{2.5}: Insights from long-term online measurements, *Sci. Total Environ.*, 814, 151954,
807 <https://doi.org/10.1016/j.scitotenv.2021.151954>, 2022c.
- 808 Zeng, J. and He, Q.: Does industrial air pollution drive health care expenditures? Spatial evidence from China, *J.*
809 *Clean. Prod.*, 218, 400–408, <https://doi.org/10.1016/j.jclepro.2019.01.288>, 2019.
- 810 Zhang, Q., Zheng, Y., Tong, D., Shao, M., Wang, S., Zhang, Y., Xu, X., Wang, J., He, H., Liu, W., Ding, Y., Lei, Y.,
811 Li, J., Wang, Z., Zhang, X., Wang, Y., Cheng, J., Liu, Y., Shi, Q., Yan, L., Geng, G., Hong, C., Li, M., Liu, F.,
812 Zheng, B., Cao, J., Ding, A., Gao, J., Fu, Q., Huo, J., Liu, B., Liu, Z., Yang, F., He, K., and Hao, J.: Drivers of
813 improved PM_{2.5} air quality in China from 2013 to 2017, *Proc. Natl. Acad. Sci. U.S.A.*, 116, 24463–24469,
814 <https://doi.org/10.1073/pnas.1907956116>, 2019.
- 815 Zhang, Y., Vu, T. V., Sun, J., He, J., Shen, X., Lin, W., Zhang, X., Zhong, J., Gao, W., Wang, Y., Fu, T. M., Ma, Y., Li,
816 W., and Shi, Z.: Significant changes in chemistry of fine particles in wintertime Beijing from 2007 to 2017:
817 Impact of Clean Air Actions, *Environ. Sci. Technol.*, 54, 1344–1352, <https://doi.org/10.1021/acs.est.9b04678>,
818 2020.
- 819 Zhang, Z., Gao, J., Zhang, L., Wang, H., Tao, J., Qiu, X., Chai, F., Li, Y., and Wang, S.: Observations of biomass
820 burning tracers in PM_{2.5} at two megacities in North China during 2014 APEC summit, *Atmos. Environ.*, 169,
821 54–64, <https://doi.org/10.1016/j.atmosenv.2017.09.011>, 2017.
- 822 Zhao, P., Feng, Y., Zhu, T., and Wu, J.: Characterizations of resuspended dust in six cities of North China, *Atmos.*
823 *Environ.*, 40, 5807–5814, <https://doi.org/10.1016/j.atmosenv.2006.05.026>, 2006.
- 824 Zhao, S., Tian, H., Luo, L., Liu, H., Wu, B., Liu, S., Bai, X., Liu, W., Liu, X., Wu, Y., Lin, S., Guo, Z., Lv, Y., and
825 Xue, Y.: Temporal variation characteristics and source apportionment of metal elements in PM_{2.5} in urban
826 Beijing during 2018–2019, *Environ. Pollut.*, 268, 115856, <https://doi.org/10.1016/j.envpol.2020.115856>, 2021.
- 827 Zheng, G., Duan, F., Ma, Y., Zhang, Q., Huang, T., Kimoto, T., Cheng, Y., Su, H., and He, K.: Episode-Based
828 Evolution Pattern Analysis of Haze Pollution: Method Development and Results from Beijing, China, *Environ.*
829 *Sci. Technol.*, 50, 4632–4641, <https://doi.org/10.1021/acs.est.5b05593>, 2016.



830 Zhang, R., Jing, J., Tao, J., Hsu, S.-C., Wang, G., Cao, J., Lee, C. S. L., Zhu, L., Chen, Z., Zhao, Y., and Shen, Z.:
 831 Chemical characterization and source apportionment of PM_{2.5} in Beijing: seasonal perspective, *Atmos. Chem.*
 832 *Phys.*, 13, 7053–7074, <https://doi.org/10.5194/acp-13-7053-2013>, 2013.

833 Zheng, M., Wang, Y., Yuan, L., Chen, N., and Kong, S.: Ambient observations indicating an increasing effectiveness
 834 of ammonia control in wintertime PM_{2.5} reduction in Central China, *Sci. Total Environ.*, 824, 153708,
 835 <https://doi.org/10.1016/j.scitotenv.2022.153708>, 2022.

836 Zhou, W., Lei, L., Du, A., Zhang, Z., Li, Y., Yang, Y., Tang, G., Chen, C., Xu, W., Sun, J., Li, Z., Fu, P., Wang, Z.,
 837 and Sun, Y.: Unexpected increases of severe haze pollution during the post COVID - 19 Period: Effects of
 838 emissions, meteorology, and secondary production, *J. Geophys. Res.-Atmos.*, 127,
 839 <https://doi.org/10.1029/2021JD035710>, 2022.

840 Ziemann, P. J. and Atkinson, R.: Kinetics, products, and mechanisms of secondary organic aerosol formation, *Chem.*
 841 *Soc. Rev.*, 41, 6582, <https://doi.org/10.1039/c2cs35122f>, 2012.

842

843

844 **Table 1.** Meteorological conditions, gas pollutants, chemical composition, and source contribution of PM_{2.5} during
 845 pollution episodes in Xi'an, Shijiazhuang, and Beijing

Parameters	Xi'an		Shijiazhuang			Beijing		
	EP1	EP2	EP3	EP4	EP5	EP6	EP7	EP8
T (°C)	4.9 ± 2.6	1.5 ± 3.5	0.4 ± 3.4	-0.2 ± 3.3	-2.7 ± 3.3	0.3 ± 3.2	-1.6 ± 3.3	5.1 ± 3.6
RH (%)	52 ± 10	45 ± 10	61 ± 15	40 ± 13	75 ± 11	57 ± 19	45 ± 24	36 ± 10
WS (m s ⁻¹)	0.5 ± 0.2	0.7 ± 0.3	1.4 ± 0.6	1.9 ± 0.8	1.4 ± 0.7	1.0 ± 0.6	1.1 ± 0.6	1.0 ± 0.6
Dominant WD ^a	WSW, WNW	WSW	NNW	NNW	NNW	NNE	NNW, NNE	NNE, ENE
CO (mg m ⁻³)	1.39 ± 0.40	1.15 ± 0.56	1.47 ± 0.62	0.60 ± 0.30	0.43 ± 0.33	1.04 ± 0.56	0.81 ± 0.32	1.00 ± 0.55
SO ₂ (μg m ⁻³)	15 ± 3	15 ± 5	9 ± 4	8 ± 4	3 ± 1	6 ± 5	4 ± 3	6 ± 4
NO ₂ (μg m ⁻³)	74 ± 22	63 ± 32	63 ± 14	47 ± 21	27 ± 11	54 ± 22	46 ± 17	42 ± 21
O _x (ppm)	47 ± 8	42 ± 10	36 ± 7	32 ± 6	27 ± 3	36 ± 6	33 ± 4	43 ± 9
ALWC (μg m ⁻³)	15 ± 11	8 ± 8	42 ± 37	12 ± 11	59 ± 448	28 ± 47	23 ± 8	11 ± 13
Dominant	OA (38%)	OA (34%)	NO ₃ ⁻ (27%)	OA (30%)	NO ₃ ⁻ (32%)	OA (32%)	OA (32%)	OA (40%)
Chemical composition	NO ₃ ⁻ (24%)	NO ₃ ⁻ (24%)	OA (26%)	NO ₃ ⁻ (23%)	OA (26%)	NO ₃ ⁻ (26%)	NO ₃ ⁻ (26%)	NO ₃ ⁻ (23%)
Dominant source contribution ^b	BB (30%) SNpS (25%) CC (17%)	SNpS (34%) BB (24%) VE (16%)	SNpS (39%) BB (23%) CC (16%)	BB (40%) CC (16%) VE (16%)	SNpS (70%) BB (16%)	SNpS (62%) BB (13%)	SNpS (61%) BB (14%)	BB (38%) SNpS (27%) VE (15%)

846 ^a WSW : west-southwest; WNW : west-northwest; NNW : north-northwest; NNE : north-northeast; ENE : East-northeast

847 ^b BB: biomass burning; SNpS: secondary nitrate plus sulfate; CC: coal combustion; VE: vehicle emission

848



849 **Figure captions:**

850 **Figure 1.** Chemical composition and source apportionment results of PM_{2.5} in three pilot cities of northern China
851 during the sampling period.

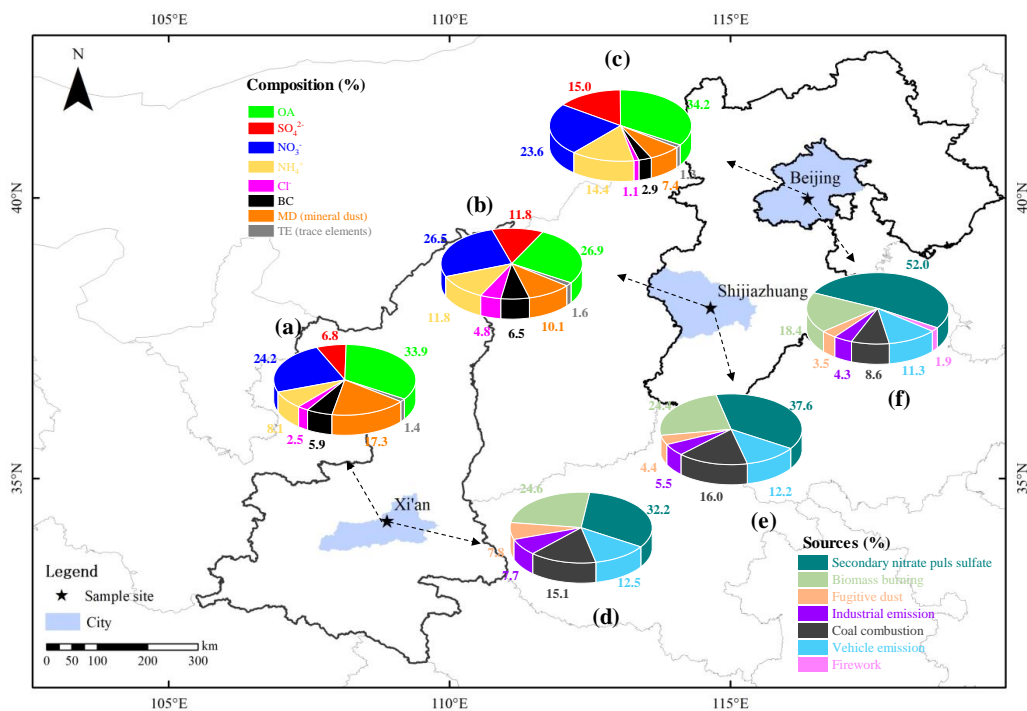
852 **Figure 2.** Mass fractions of chemical components (a-c) and sources contribution (d-f) with reconstructed PM_{2.5}
853 concentration in Xi'an, Shijiazhuang, and Beijing.

854 **Figure 3.** Correlations of secondary nitrate plus sulfate/ Δ CO and O_x mixing ratio in (a) Xi'an, (b) Shijiazhuang, and
855 (c) Beijing. Each point and its error bar represent the mean and standard deviation in each bin (Δ O_x = 5 ppb).

856 **Figure 4.** Correlation of secondary nitrate plus sulfate/ Δ CO and ALWC during winter in (a) Xi'an, (b) Shijiazhuang,
857 and (c) Beijing, respectively. The points and error bar represent the mean values and standard deviation values of
858 secondary nitrate plus sulfate/ Δ CO and O_x in each bin. In Xi'an, each bin is 5 $\mu\text{g m}^{-3}$ (Δ ALWC = 5 $\mu\text{g m}^{-3}$). In
859 Shijiazhuang, each bin is 5 $\mu\text{g m}^{-3}$ (Δ ALWC = 5 $\mu\text{g m}^{-3}$) when ALWC ranged from 0 to 75 $\mu\text{g m}^{-3}$, but 25 $\mu\text{g m}^{-3}$
860 (Δ ALWC = 25 $\mu\text{g m}^{-3}$) for ALWC ranged from 75 to 200 $\mu\text{g m}^{-3}$ due to limitations in data. In Beijing, each bin is 5
861 $\mu\text{g m}^{-3}$ (Δ ALWC = 5 $\mu\text{g m}^{-3}$) when ALWC ranged from 0 to 50 $\mu\text{g m}^{-3}$, but 100 $\mu\text{g m}^{-3}$ (Δ ALWC = 100 $\mu\text{g m}^{-3}$) for
862 ALWC ranged from 50 to 900 $\mu\text{g m}^{-3}$ due to limitations in data.

863 **Figure 5.** Summary of PM_{2.5} and its composition (a, b, c) and source contribution (d, e, f) in Xi'an, Shijiazhuang,
864 and Beijing in winter in past decades. Where * represents the result of this study. The data and references used for
865 this figure are listed in Table S5 and S7.

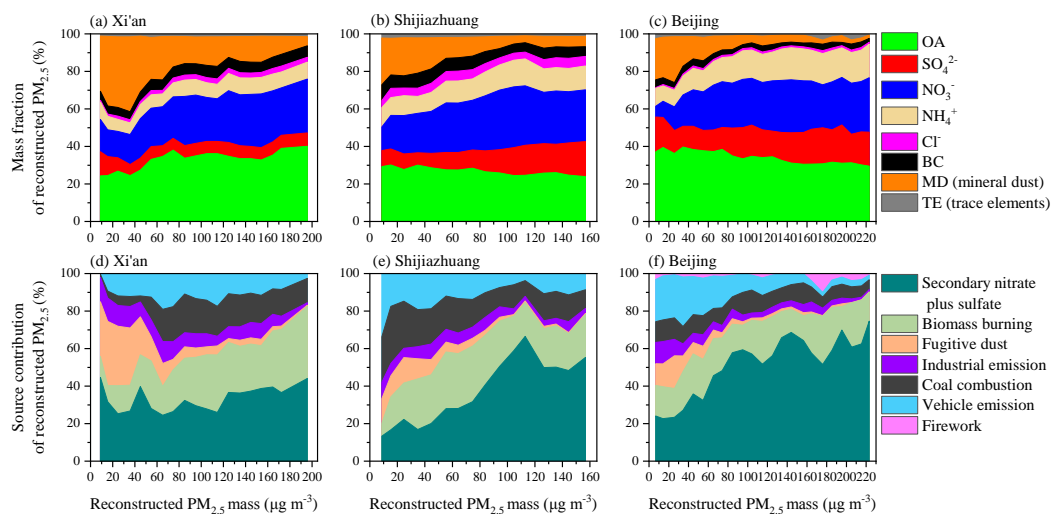
866



867

868 **Figure 1.** Chemical composition and source apportionment results of PM_{2.5} in three pilot cities of northern China
 869 during the sampling period.

870



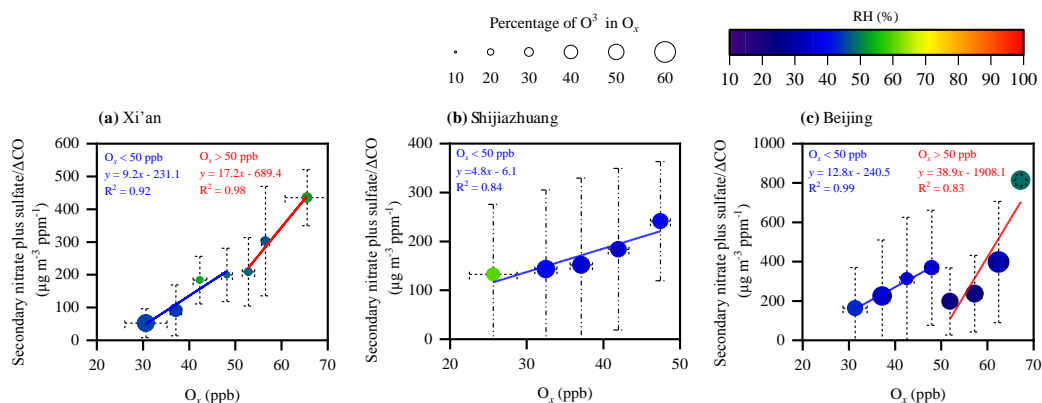
871

872

873

874

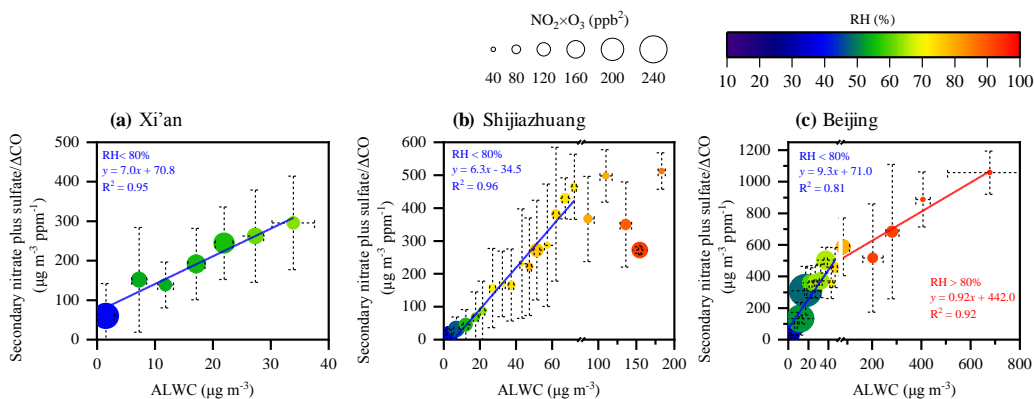
Figure 2. Mass fractions of chemical components (a-c) and sources contribution (d-f) with reconstructed $PM_{2.5}$ concentration in Xi'an, Shijiazhuang, and Beijing.



875

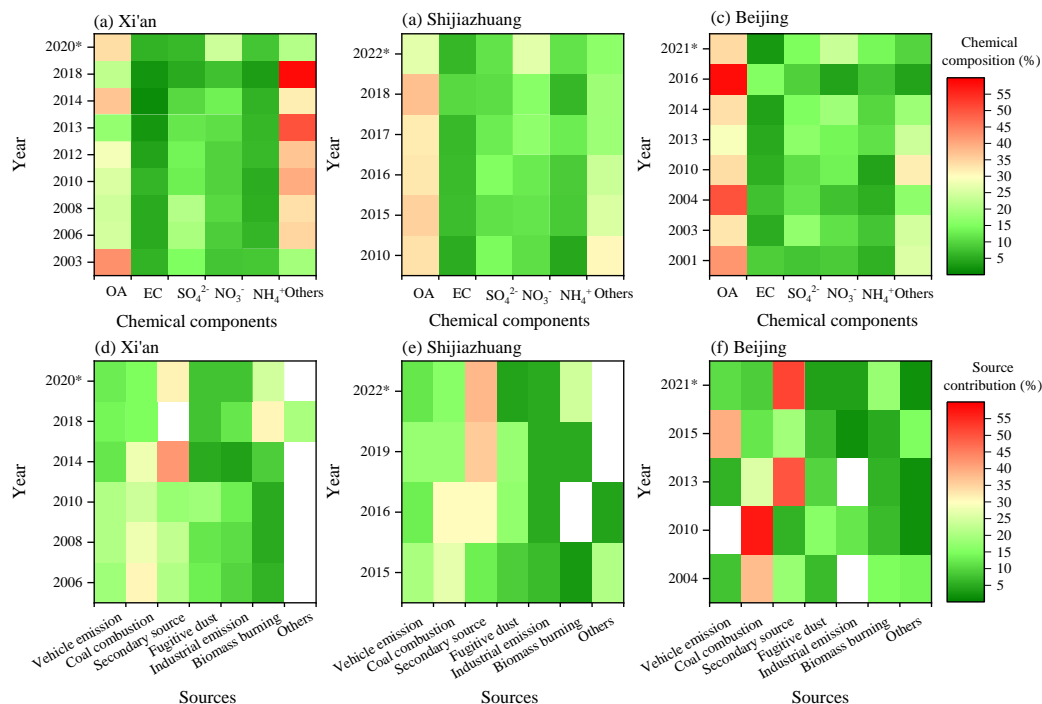
876 **Figure 3.** Correlations of secondary nitrate plus sulfate/ΔCO and O_x mixing ratio in (a) Xi'an, (b) Shijiazhuang, and
877 (c) Beijing. Each point and its error bar represent the mean and standard deviation in each bin ($\Delta\text{O}_x = 5$ ppb).

878



879

880 **Figure 4.** Correlation of secondary nitrate plus sulfate/ΔCO and ALWC during winter in (a) Xi'an, (b) Shijiazhuang,
881 and (c) Beijing, respectively. The points and error bar represent the mean values and standard deviation values of
882 secondary nitrate plus sulfate/ΔCO and O_x in each bin. In Xi'an, each bin is $5 \mu\text{g m}^{-3}$ ($\Delta\text{ALWC} = 5 \mu\text{g m}^{-3}$). In
883 Shijiazhuang, each bin is $5 \mu\text{g m}^{-3}$ ($\Delta\text{ALWC} = 5 \mu\text{g m}^{-3}$) when ALWC ranged from 0 to $75 \mu\text{g m}^{-3}$, but $25 \mu\text{g m}^{-3}$
884 ($\Delta\text{ALWC} = 25 \mu\text{g m}^{-3}$) for ALWC ranged from 75 to $200 \mu\text{g m}^{-3}$ due to limitations in data. In Beijing, each bin is 5
885 $\mu\text{g m}^{-3}$ ($\Delta\text{ALWC} = 5 \mu\text{g m}^{-3}$) when ALWC ranged from 0 to $50 \mu\text{g m}^{-3}$, but $100 \mu\text{g m}^{-3}$ ($\Delta\text{ALWC} = 100 \mu\text{g m}^{-3}$) for
886 ALWC ranged from 50 to $900 \mu\text{g m}^{-3}$ due to limitations in data.



887

888 **Figure 5.** Summary of PM_{2.5} and its composition (a, b, c) and source contribution (d, e, f) in Xi'an, Shijiazhuang,
 889 and Beijing in winter in past decades. Where * represents the result of this study, and the empty white area means no
 890 data. The data and references used for this figure are listed in Table S6 and S7.

891